Supplement of Atmos. Chem. Phys., 15, 6351–6366, 2015
http://www.atmos-chem-phys.net/15/6351/2015/
doi:10.5194/acp-15-6351-2015-supplement

Atmospheric Chemistry and Physics Open Access

Supplement of

Investigating the annual behaviour of submicron secondary inorganic and organic aerosols in London

D. E. Young et al.

Correspondence to: H. Coe (hugh.coe@manchester.ac.uk)

1 NR-PM_1 data quality assurance

1.1 Relative Ionisation Efficiencies (RIEs)

	NH_4	SO_4
cToF-AMS long-term	3.8455	1.1379
HR-ToF-AMS winter IOP	2.9875	1.2
HR-ToF-AMS summer IOP	3.272	1.4809

Table S1. RIE values for ammonium and sulphate calculated from ammonium nitrate and ammonium sulphate calibrations of the cToF-AMS and HR-ToF-AMS. Ammonium sulphate calibrations of the HR-ToF-AMS were only performed during the summer IOP and so the default RIE for sulphate (1.2) is applied in the winter IOP. The RIEs calculated are the average values from all available calibrations for each of the IOPs for the HR-ToF-AMS and from the whole measurement period for the cToF-AMS.

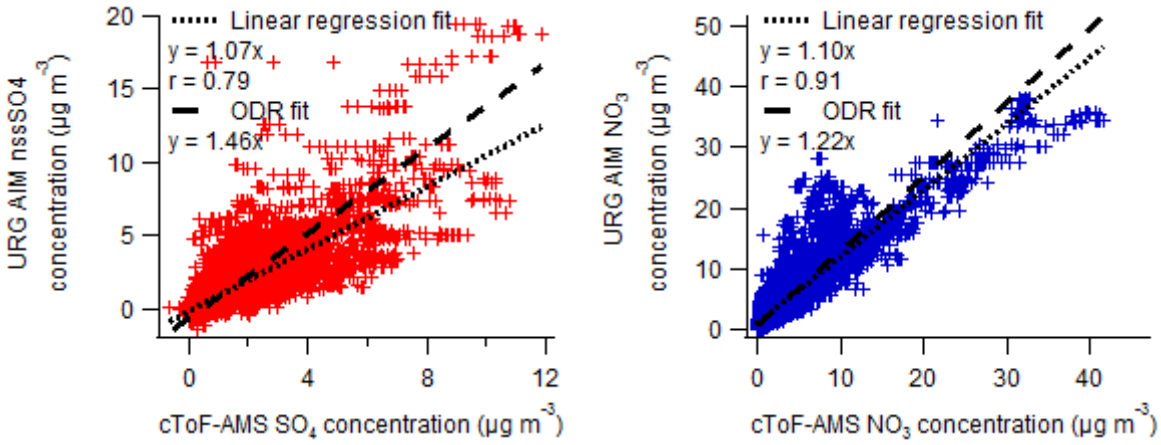

Figure S1. Left: Comparison of the sulphate concentration from the cToF-AMS (corrected using the RIEs in Table S1) with the calculated concentration of non-sea salt sulphate from the URG-9000B Ambient Ion Monitor (AIM) at North Kensington (PM_{10}) for the full calendar year. Right: Comparison of the nitrate concentrations between the cToF-AMS and URG AIM for the full calendar year. The data are fitted using both linear and orthogonal distance regressions (ODR).

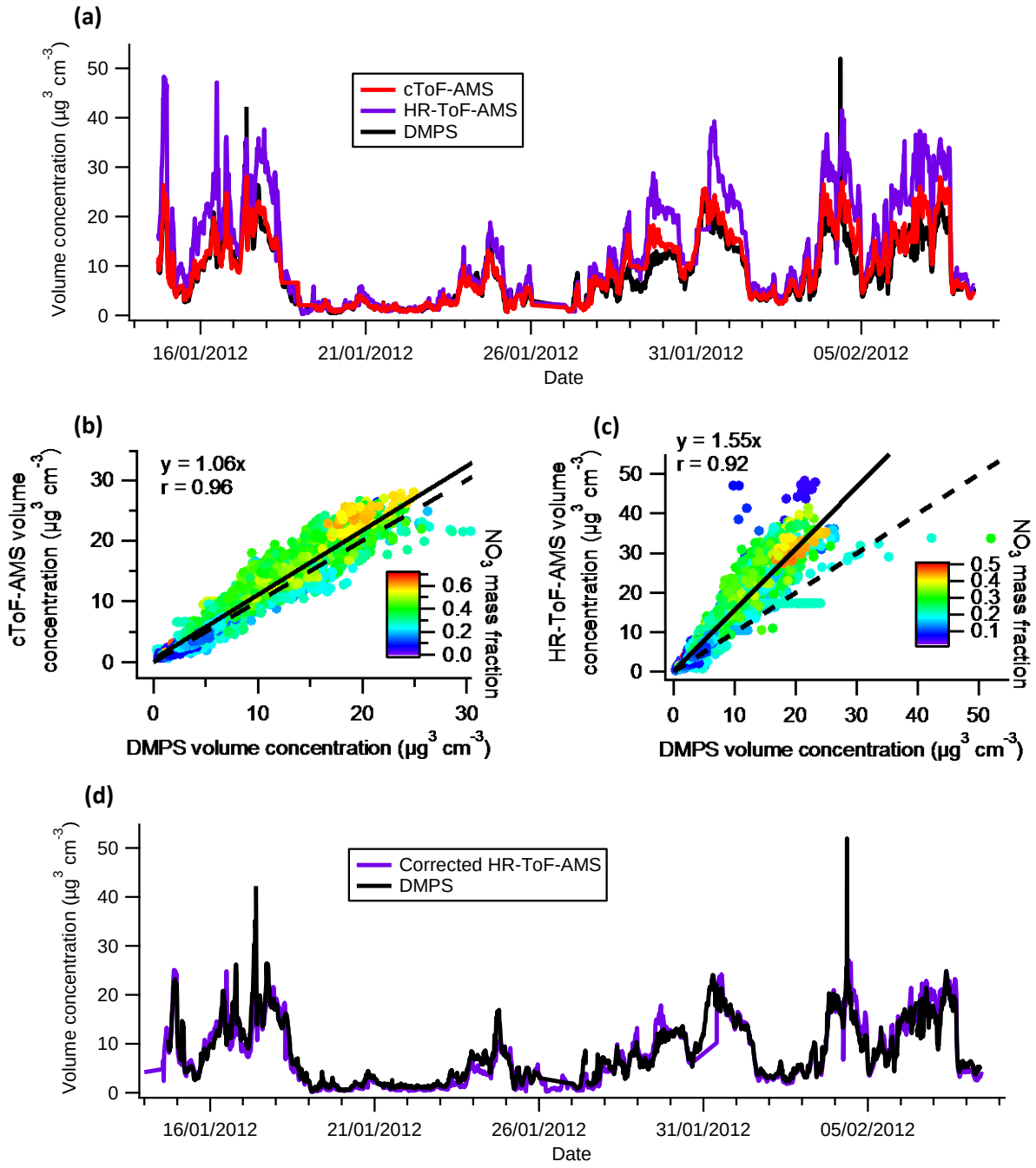

Figure S2. (a) Volume concentration comparison between the DMPS and the two AMS instruments for the winter IOP. Densities of 1.27 and 1.77 g cm^{-3} (reported by Cross et al., 2007) for organic and inorganic contributions, respectively, were assumed for estimating the AMS volume concentrations. (b) Correlation of the volume concentrations for the cToF-AMS and DMPS, coloured as a function of nitrate mass fraction. (c) Correlation of the volume concentrations of the HR-ToF-AMS and DMPS coloured as a function of nitrate mass fraction. (d) Time series of the volume concentrations of the DMPS and HR-ToF-AMS data where the HR-ToF-AMS concentrations of all species but nitrate have been scaled by 0.5 for the winter IOP following the previous volume concentration comparisons.

1.2 Changes in flow rate

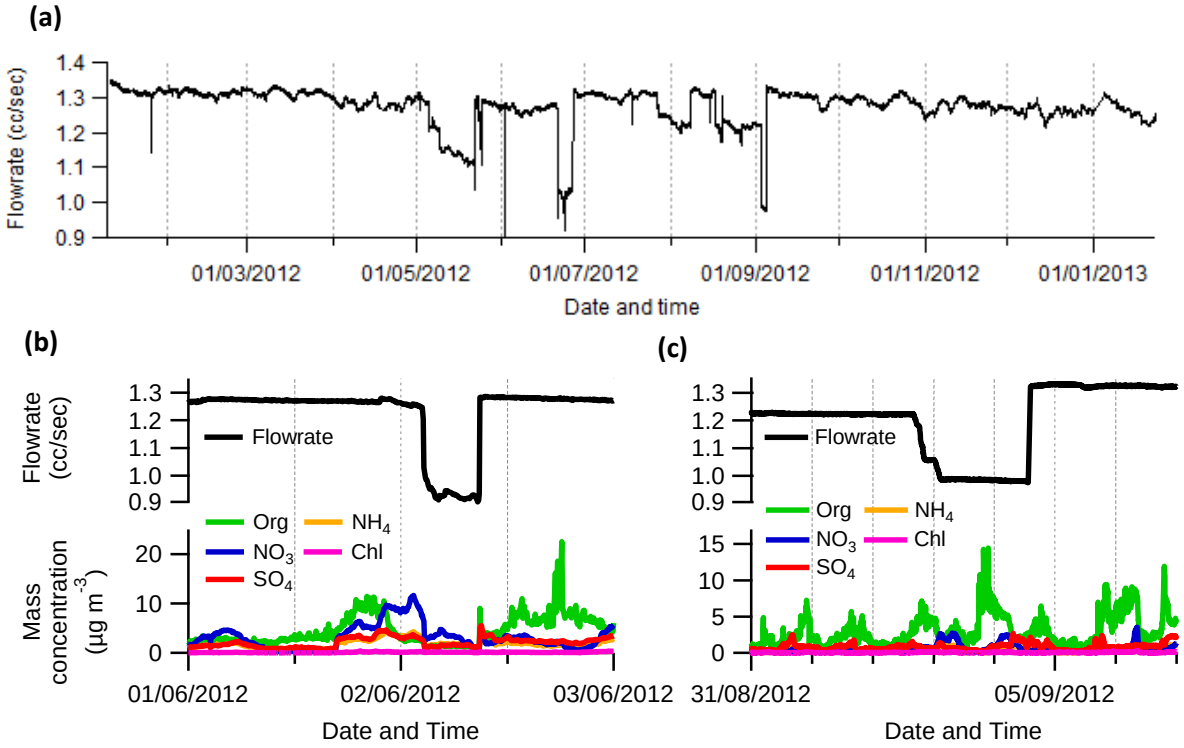

Figure S3. (a) Time series of the flow rate. (b) Step change in mass concentration concurrent with a step change in the flow rate. These data were removed from further analyses. (c) No obvious change in the mass concentration associated with a step change in the flow rate.

2 cToF-AMS vs. HR-ToF-AMS concentrations

2.1 Winter IOP

The HR-ToF-AMS sulphate RIE during the winter IOP was ambiguous as a sulphate calibration was not performed during this measurement period. The HR-ToF-AMS concentrations were compared to those of the cToF-AMS, which was calibrated later during the campaign. The slopes from the linear and ODR fits indicated that the HR-ToF-AMS concentrations were approximately double that of the cToF-AMS. The concentrations of all the HR-ToF-AMS species except nitrate were scaled by 0.5.

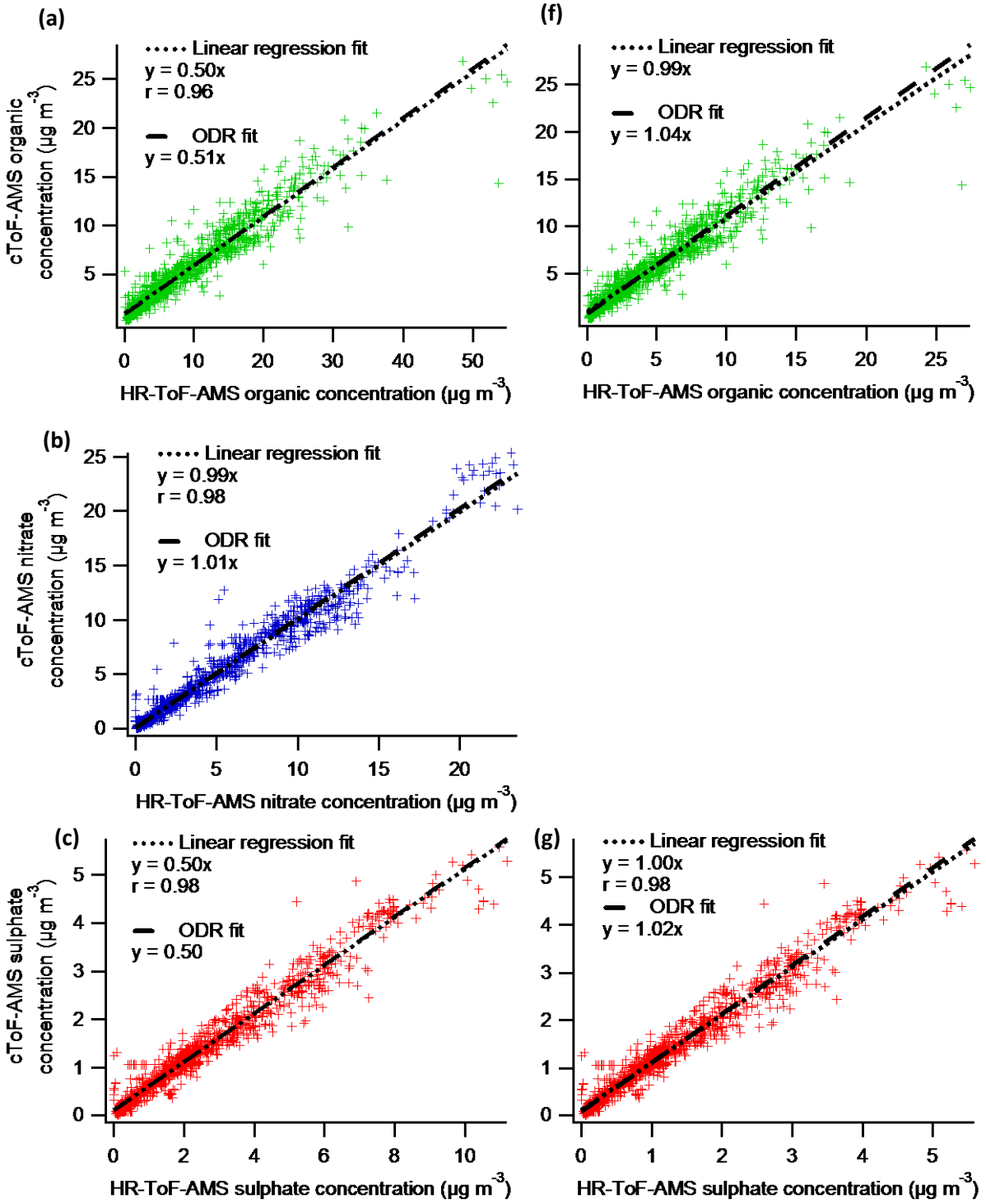
(a)
Linear regression fit
y = 0.50x
r = 0.96
ODR fit
y = 0.51x
cToF-AMS organic concentration (µg m-3)
HR-ToF-AMS organic concentration (µg m-3)
(f)
Linear regression fit
y = 0.99x
ODR fit
y = 1.04x
HR-ToF-AMS organic concentration (µg m-3)
(b)
Linear regression fit
y = 0.99x
r = 0.98
ODR fit
y = 1.01x
cToF-AMS nitrate concentration (µg m-3)
HR-ToF-AMS nitrate concentration (µg m-3)
(c)
Linear regression fit
y = 0.50x
r = 0.98
ODR fit
y = 0.50
cToF-AMS sulphate concentration (µg m-3)
HR-ToF-AMS sulphate concentration (µg m-3)
(g)
Linear regression fit
y = 1.00x
r = 0.98
ODR fit
y = 1.02x
HR-ToF-AMS sulphate concentration (µg m-3)

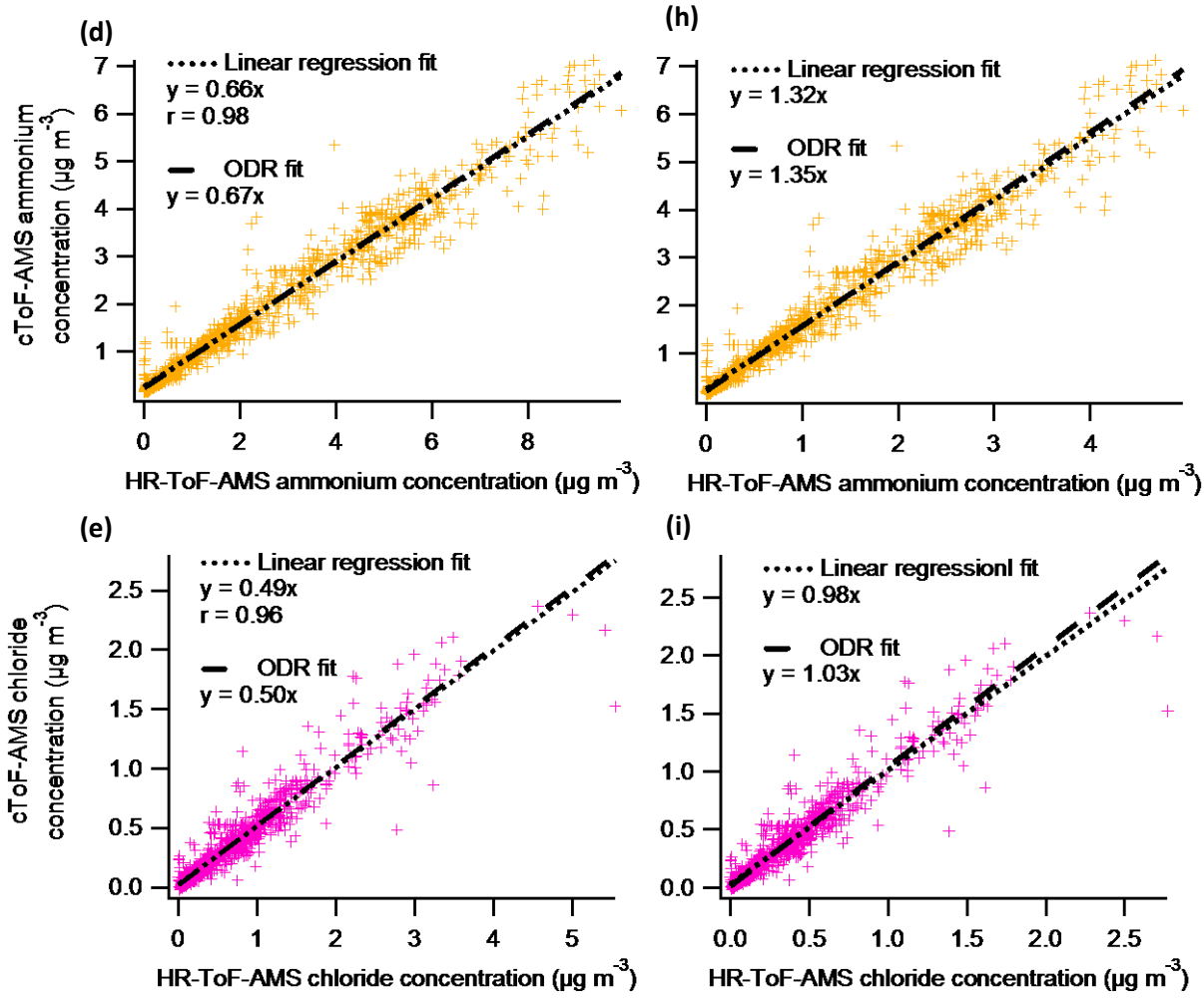

Figure S4. Correlation of the time series of NR-PM_1 species between the cToF-AMS and HR-ToF-AMS for the winter IOP: (a-e) uncorrected concentrations, (f-i) corrected concentrations whereby the concentrations of all HR-ToF-AMS species except nitrate are scaled by 0.5.

2.2 Summer IOP

Sulphate calibrations were performed on the HR-ToF-AMS during the summer IOP, where the resulting concentrations were very similar and compared strongly with those of the cToF-AMS for the same period.

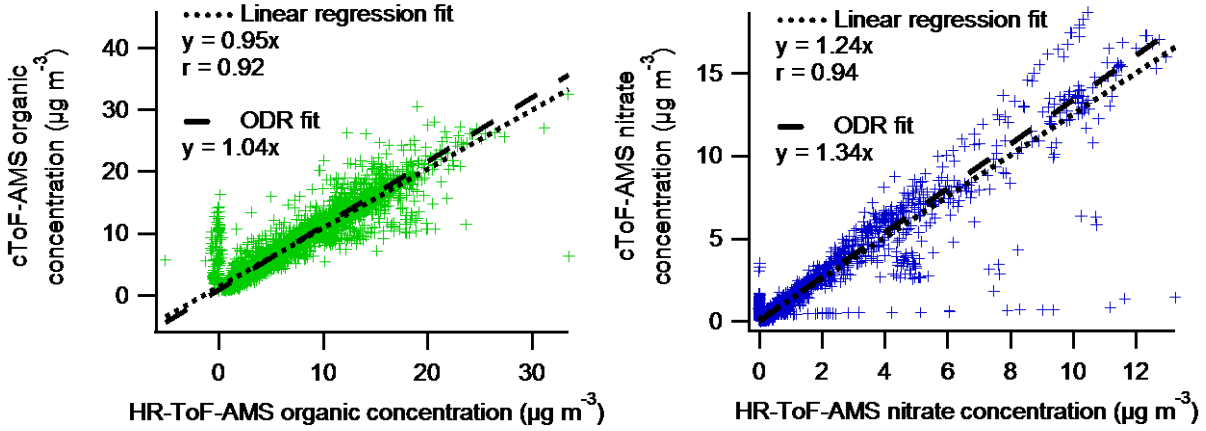

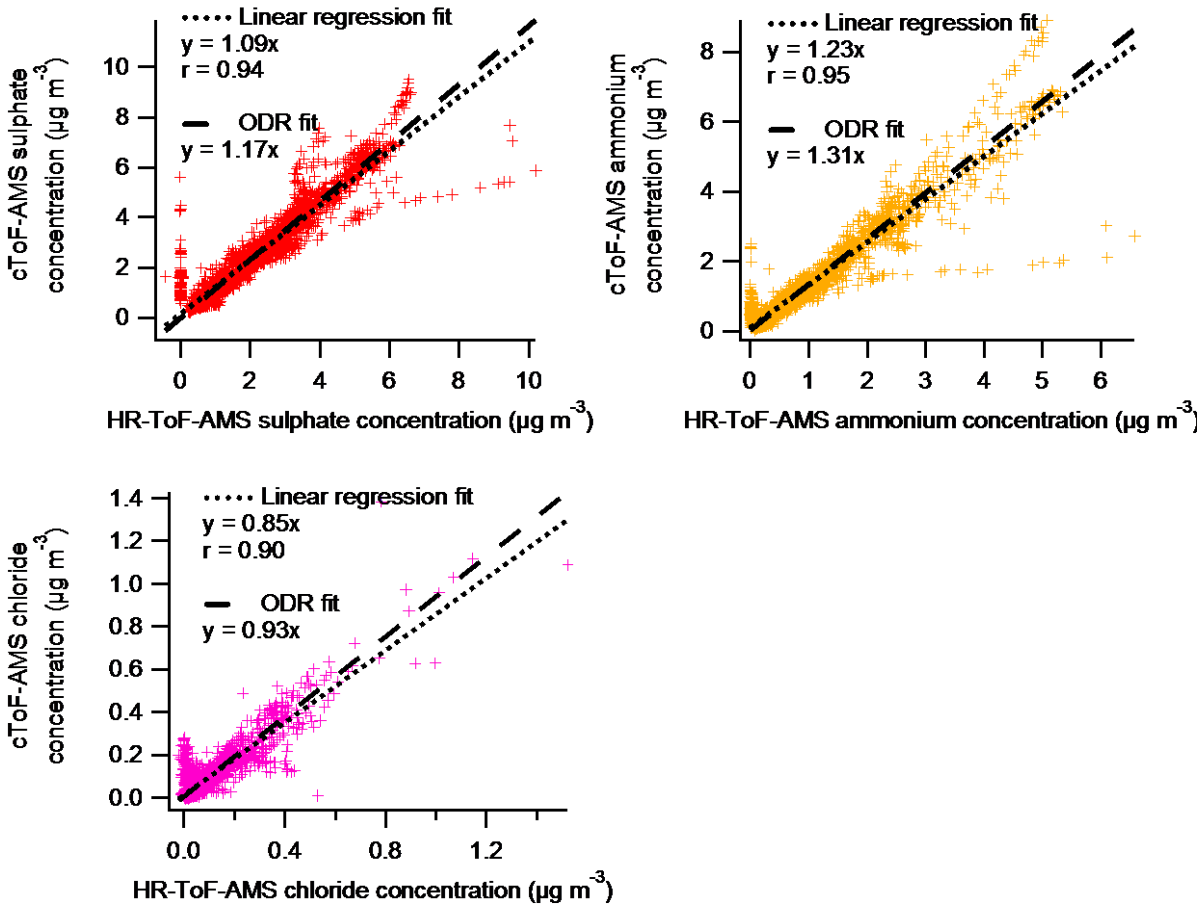

Figure S5. Correlation of the time series of NR-PM_1 species between the cToF-AMS and HR-ToF-AMS for the summer IOP.

3 cToF-AMS NR-PM_1 supplementary

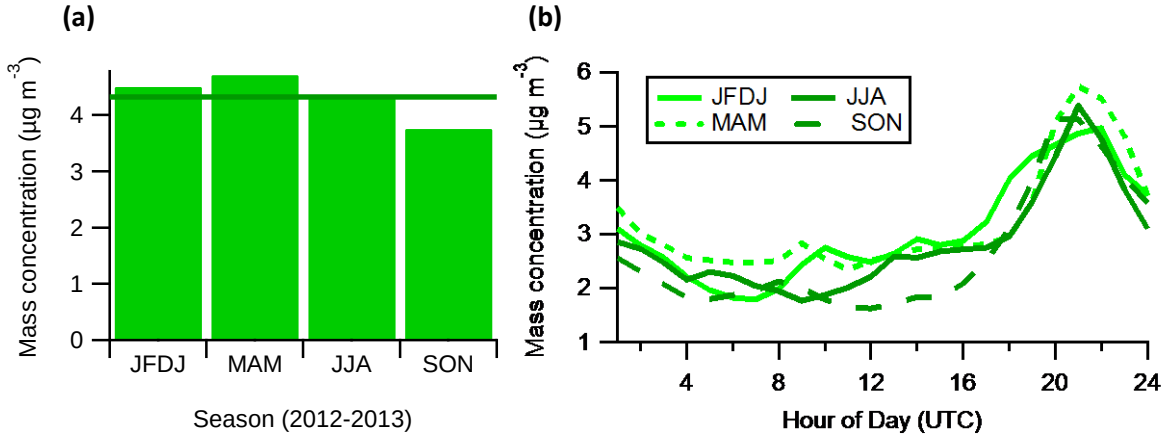

Figure S6. (a) Avearge organic seasonal mass bar chart. Thick line denotes annual average organic mass (b) Median organic diurnal profiles for each of the seasons.

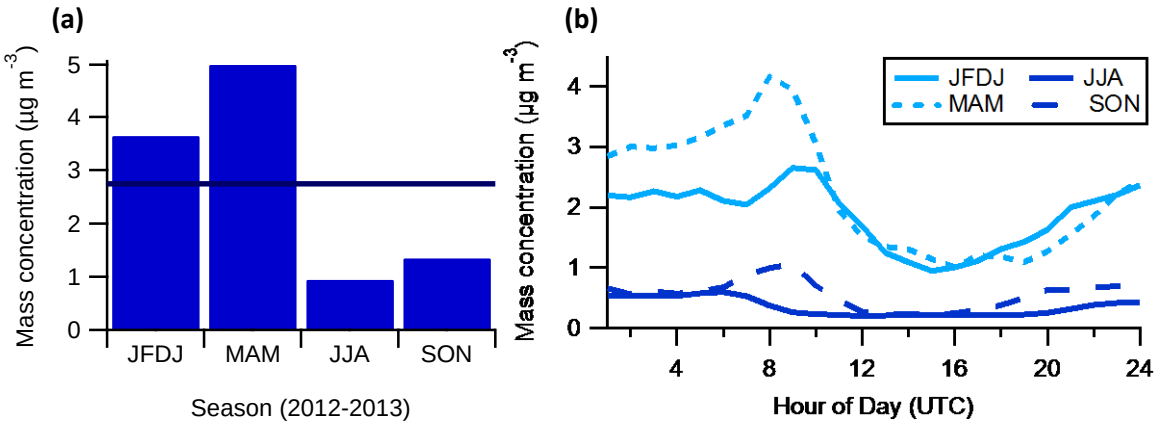

Figure S7. (a) Avearge nitrate seasonal mass bar chart. Thick line denotes annual average nitrate mass. (b) Median nitrate diurnal profiles for each of the seasons.

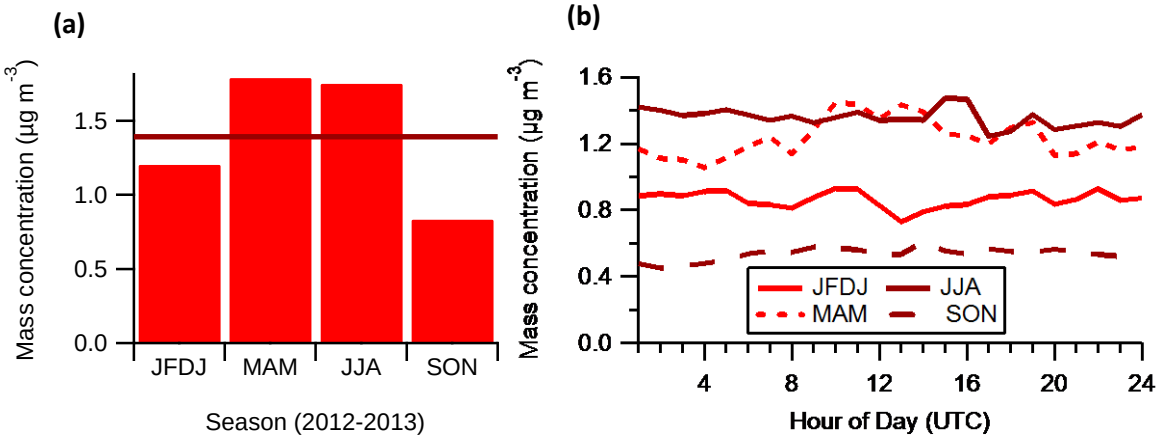

Figure S8. (a) Avearge sulphate seasonal mass bar chart. Thick line denotes annual average sulphate mass. (b) Median sulphate diurnal profiles for each of the seasons.

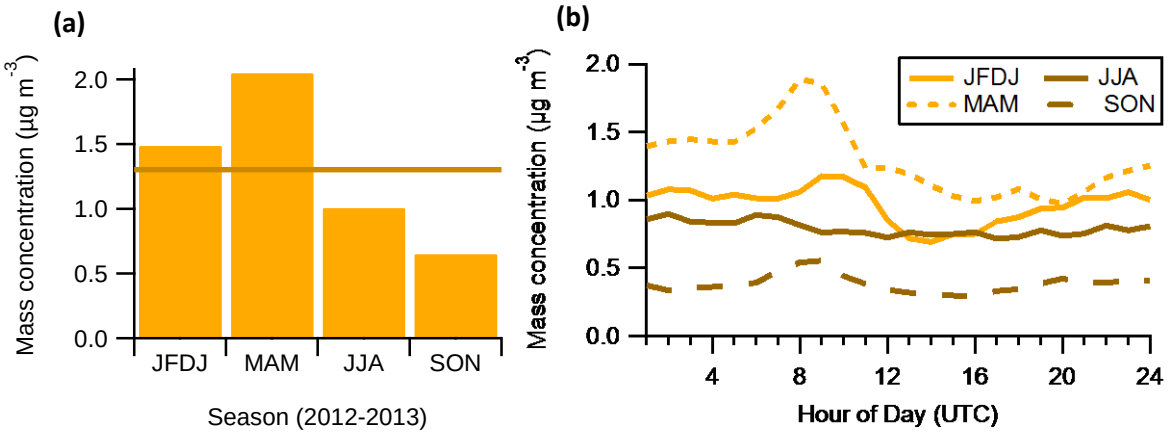

Figure S9. (a) Avearge ammonium seasonal mass bar chart. Thick line denotes annual average ammonium mass. (b) Median ammonium diurnal profiles for each of the seasons.

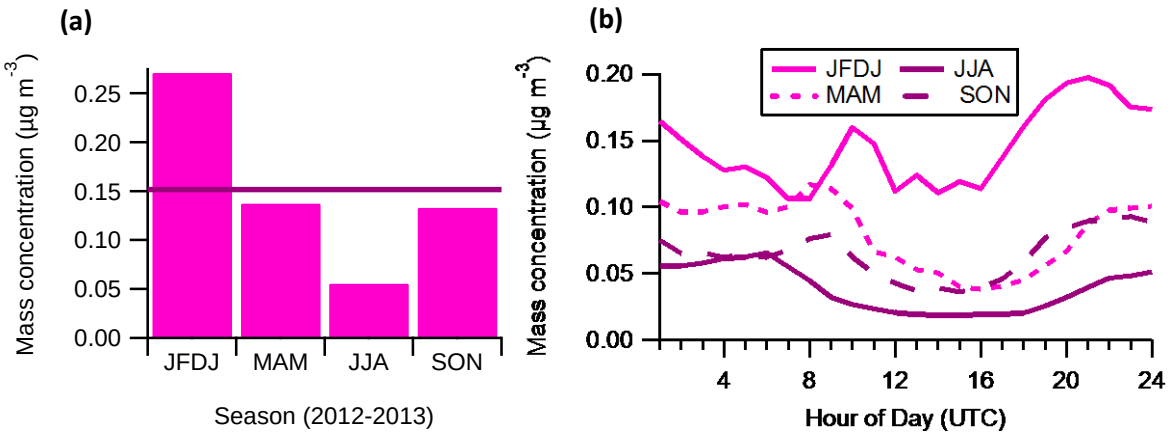

Figure S10. (a) Avearge chloride seasonal mass bar chart. Thick line denotes annual average chloride mass. (b) Median chloride diurnal profiles for each of the seasons.

4 cToF-AMS PMF supplementary

4.1 Data preparation methods

Positive matrix factorisation (PMF) was applied to the organic aerosol data from the cToF-AMS. The data were prepared in the recommended method of practice as described by Ulbrich et al. (2009) and the resulting matrix consisted of m/z's 12-150. Any "bad" ions with a signal to noise ratio less than 0.2 were removed from the data and error matrices before PMF analysis (Ulbrich et al., 2009; Paatero and Hopke, 2003). Ions with a signal to noise ratio of less than 2 were deemed 'weak' and downweighted by a factor of 2. Downweighting was performed to reduce the influence of some signals to the PMF solution in order to avoid PMF trying to explain the noise. Those peaks related to the CO_2^+ ion (m/z 44) were also downweighted, or rather 'not upweighted', to reduce the influence from duplicated ions to the signal.

Several criteria are used to select the appropriate number of factors, as this is the most subjective part of PMF analysis. Firstly, there are diagnostics within the PMF analysis toolkit, which can be used to assess the quality and suitability of a solution set. For example, the mathematical criterion Q determines the quality of fit of the data that is minimised through an iterative least squares fit of the PMF solution for the chosen number of factors. Q is defined as the sum of the weighted residuals divided by the standard deviations of the points in the data matrix. If the value of $Q/Q_{expected}$ is 1 then the model is appropriate and the estimation of the data uncertainties are accurate thus the solution set accounts for the variance associated with random errors. An underestimation of the errors in the data i.e. variance unaccounted for by the solution set, is indicated by values of $Q/Q_{expected}$ greater than 1. However, the solution set that is atmospherically realistic and the solution set with the number of factors resulting in a value of $Q/Q_{expected}$ closest to unity may not be the same. Therefore, the solution is validated with external parameters, both reference mass spectra and other measurement parameters. Furthermore, the fPeak parameter is used to explore ambiguity in the solution due to rotational freedom, a known problem with factor analyses (Paatero et el., 2002). Random initial values, or seeds, can also be used to explore the stability of a solution.

The reference mass spectra used in this discussion are from the AMS spectral database. The individual spectra used are referenced appropriately. Unit mass resolution (UMR) database: Ulbrich, I.M., Lechner, M., and Jimenez, J.L. AMS Spectral Database. URL: http://cires.colorado.edu/jimenez-

group/AMSsd/. Details of the databases are described in Ulbrich et al. (2009). Ancillary data used for correlations between PMF factors are from other measurements made during the relevant measuring campaign from the Manchester group such as the NO_3, SO_4, NH_4 masses. CO and NO_x have been provided by James Lee from the University of York and David Green from Kings College London, respectively. Note that the CO data only covers the period January-August inclusive.

In Section 4.2, the methods used to identify and remove a period of problematic data around the summer IOP are outlined. In Section 4.3, the different cToF-AMS PMF solution sets are explored and the criteria used for choosing the final solution set are discussed. In Section 5, the HR-ToF-AMS PMF analysis is outlined where the different solution sets and criteria for choosing the final solution for the winter IOP and summer IOP are explored in Sections 5.1 and 5.2, respectively. Finally, in Section 6, the mass spectra and time series of the final solutions from the cToF-AMS and the HR-ToF-AMS PMF are compared where possible.

For the year-long cToF-AMS data set, a 5-factor solution was chosen, where the five factors were identified as HOA, COA, SFOA, OOA1, and OOA2.

4.2 Exclusion of data during summer period

PMF was run on the organic matrix from the entire year of data (PMF_{full}). When the time series of the chosen five-factor solution were looked at in detail, a step change in the data was apparent between 20 July and 24 August 2012. This sudden (20-60 minutes including down time) increase in concentration resulted in the masses being approximately an order of magnitude greater than those of the period preceding the step change. This was most evident in the time series of factors 3 (OOA1), 5 (HOA), and possibly factor 4 (SFOA). Diagnostics in the main Squirrel analysis toolkit highlighted a simultaneous step change in the heater bias.

A change in the instrument's tuning was identified as being the cause for these changes. When the AMS was set up in January 2012, it was known that it would continue to be run at least until the end of the summer IOP. The instrument was therefore essentially 'detuned' in order to prolong the life of several components such as the MCP. At the start of the summer IOP the instrument was tuned and these settings were not returned to their original 'detuned' state until a month later (19 August). Furthermore, there were some variations in the concentrations and heater bias between 19 and 24 August, so this period was also questionable. However, these step changes in the data are only evident after PMF is applied whereby the total organic concentrations in this summer period are comparable to if not less than that of other events such as the one in May. This is also the case for org44 and other AMS species.

In order to evaluate the extent to which the data were affected and determine the most suitable PMF run for further analyses, PMF was run on the data set three more times: once with the summer period removed prior to running PMF (PMF_{noSum}), once on the dataset before the summer period (PMF_{before}) and finally once with the data after the summer (PMF_{after}). The same number of factors and the same factor types were identified in all three runs.

4.2.1 Comparison of mass spectral profiles

PMF appears to be sensitive to the data matrix on which it is applied, whereby, for example, there are missing peaks in the mass spectral profiles and very small peaks in places other than the main

peaks used to identify the factors (Fig. S11). Factor 2 also contained unusually large peaks at m/z 58 and 94 in the after summer run, where m/z can be associated with amines. However, the time series of both these peaks are noisy. Factor 2 for this particular PMF run may not actually be the same factor as identified in the other PMF runs (OOA2).

Correlations between the mass spectral profiles from PMF_{full} and the three other runs were performed (Table S2), as were correlations between PMF_{noSum} with PMF_{before} and PMF_{after} (Table S3), and between the factors from PMF_{before} and PMF_{after} (Table S4).

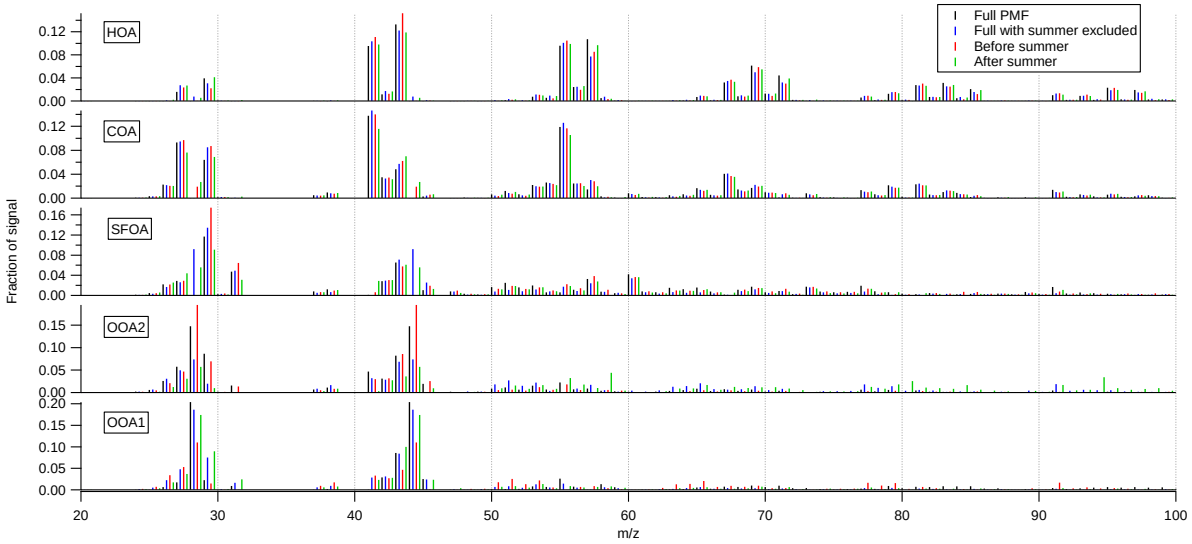

Figure S11. Mass spectra of the different factors for the different PMF runs.

Strong correlations between the mass spectra for the factors from PMF_{full} and PMF_{noSum} were found for most factors (0.72-0.99), with the highest Pearson's r values for comparisons of the COA and HOA factors and the lowest for SFOA. When the factors from PMF_{before} and PMF_{after} were compared, the weakest correlation was for SFOA (0.79). There is possibly some mixing/alternation between the two OOA subcomponents, where stronger correlations are found between OOA2 from one PMF run and OOA1 from another.

		PMF_{noSum}					PMF_{before}					PMF_{after}				
	Factor	**OOA2**	**COA**	**OOA1**	**SFOA**	**HOA**	**OOA2**	**COA**	**OOA1**	**SFOA**	**HOA**	**OOA2**	**COA**	**OOA1**	**SFOA**	**HOA**
PMF_{full}	**OOA2**	0.87	0.39	0.98	0.86	0.36	0.98	0.50	0.91	0.40	0.31	0.71	0.57	0.98	0.84	0.34
	COA	0.38	0.99	0.23	0.29	0.77	0.23	0.98	0.28	0.41	0.72	0.33	0.97	0.22	0.51	0.74
	OOA1	0.73	0.10	0.96	0.72	0.21	0.96	0.22	0.83	0.10	0.17	0.75	0.30	0.95	0.59	0.19
	SFOA	0.42	0.42	0.29	0.72	0.35	0.26	0.43	0.23	0.96	0.34	0.21	0.45	0.35	0.81	0.39
	HOA	0.33	0.73	0.19	0.30	0.98	0.19	0.73	0.16	0.37	0.98	0.30	0.74	0.24	0.43	0.99

Table S2. Comparison of the mass spectra from PMF_{full} with PMF_{noSum}, PMF_{before}, and PMF_{after}. All correlations are with PMF_{full} on the x-axis.

		PMF_{before}					PMF_{after}				
	Factor	**OOA2**	**COA**	**OOA1**	**SFOA**	**HOA**	**OOA2**	**COA**	**OOA1**	**SFOA**	**HOA**
PMF_{noSum}	**OOA2**	0.82	0.45	0.95	0.31	0.37	0.72	0.54	0.81	0.79	0.37
	COA	0.24	0.99	0.26	0.47	0.76	0.31	0.97	0.25	0.54	0.79
	OOA1	1.00	0.37	0.90	0.30	0.21	0.72	0.44	0.99	0.76	0.24
	SFOA	0.81	0.43	0.65	0.75	0.27	0.56	0.48	0.87	0.92	0.33
	HOA	0.25	0.81	0.23	0.35	0.99	0.37	0.83	0.29	0.46	0.99

Table S3. Comparison of the mass spectra from PMF_{noSum} with PMF_{before} and PMF_{after}. All correlations are with PMF_{noSum} on the x-axis.

		PMF_{after}				
	Factor	**OOA2**	**COA**	**OOA1**	**SFOA**	**HOA**
PMF_{before}	**OOA2**	0.73	0.43	0.99	0.74	0.23
	COA	0.39	0.99	0.37	0.61	0.79
	OOA1	0.73	0.44	0.87	0.71	0.21
	SFOA	0.17	0.48	0.36	0.79	0.39
	HOA	0.25	0.78	0.32	0.42	0.98

Table S4. Comparison of the mass spectra from PMF_{before} and PMF_{after}.

4.2.2 Comparison of time series

It was only possible to compare the time series from PMF_{full} with the other three runs (Table S5) and PMF_{noSum} with PMF_{before} and PMF_{after} (Table S6). As for the mass spectral profiles, the strong COA and HOA correlations and possible mixing of the OOA subtypes also holds true when comparing PMF_{full} with the three additional PMF runs and when PMF_{noSum} is compared to PMF_{before} and PMF_{after}. The correlations of the OOA1 and OOA2 time series are the weakest in all comparisons of the PMF runs. In all comparisons, the correlations of HOA, COA, and SFOA are very strong (0.95-1.00). Reducing the number of factors derived from PMF to 4, so that there is only a single OOA factor, does not resolve this issue as HOA and SFOA are still affected by the changes in instrument tuning.

A high-resolution ToF AMS was running during the summer IOP between 19 July and 19 August at the same site as the cToF-AMS although they were approximately 30m apart. As expected for the summer, an SFOA factor was not derived from the PMF run on this data set (see Section 5.2), so a correction factor could not be calculated using these outputs. The HR-ToF-AMS also operated within the period of changes in tuning of the cToF-AMS so there was no crossover period of HR-ToF-AMS measurements and unaffected cToF-AMS measurements. Furthermore, comparison of the time series of the two OOA subtypes from the cToF-AMS and the HR-ToF-AMS highlighted the rotation occurring within the SOA, especially at the beginning of the summer IOP (23-26 July). The mass is distributed between the two subtypes differently depending on the instrument. A correction factor would have to be time dependent and for particular events, which is unlikely to be reliable.

In summary, although the factor types did not change when PMF was applied to the different time periods from the cToF-AMS there is no obvious way to quantify the change in masses identified during the summer in order to apply a correction factor. If the data were used in further analyses, it would create an artefact in the way of an instrument factor rather than an ambient factor. PMF_{noSum} was therefore chosen to be the most suitable solution for further analyses where the OOA subtypes would be explored.

		PMF_{noSum}					PMF_{before}					PMF_{after}				
	Factor	**OOA2**	**COA**	**OOA1**	**SFOA**	**HOA**	**OOA2**	**COA**	**OOA1**	**SFOA**	**HOA**	**OOA2**	**COA**	**OOA1**	**SFOA**	**HOA**
PMF_{full}	**OOA2**	0.60		0.94			0.96		0.69			0.51		0.92		
	COA		0.96					0.96					0.99			
	OOA1	0.51		0.74			0.92		0.47			0.83		0.76		
	SFOA				0.97					0.95					0.99	
	HOA					0.99					1.00					1.00

Table S5. Comparison of the relevant time periods between PMF_{full} with those from PMF_{noSum}, PMF_{before}, and PMF_{after}. All correlations are with PMF_{full} on the x-axis.

		PMF_{before}					PMF_{after}				
	Factor	**OOA2**	**COA**	**OOA1**	**SFOA**	**HOA**	**OOA2**	**COA**	**OOA1**	**SFOA**	**HOA**
PMF_{noSum}	**OOA2**	0.45		0.98			0.82		0.60		
	COA		0.99					0.99			
	OOA1	0.99		0.52			0.34		0.94		
	SFOA				0.99					0.97	
	HOA					1.00					1.00

Table S6. Comparison of the relevant time periods between PMF_{noSum} with those from PMF_{before} and PMF_{after}. All correlations are with PMF_{noSum} on the x-axis.

4.3 Choosing the cToF-PMF solution set

PMF was run in the typical exploration mode, running from 4 to 7 factors and fPeaks -1 to +1 in 0.5 increments. A run of initialisation seeds 0-20 for the different factor solutions was also performed.

4.3.1 4-factor solution

Although the 4-factor solution gives a reasonable solution with a Q/Q_{exp} of 1.44208, factor 3 exhibits peaks at m/z 55 and m/z 60 (Fig. S12), which are typical marker peaks for two different sources. fPeak values between -1 and 0.5 produced solutions that could be considered valid.

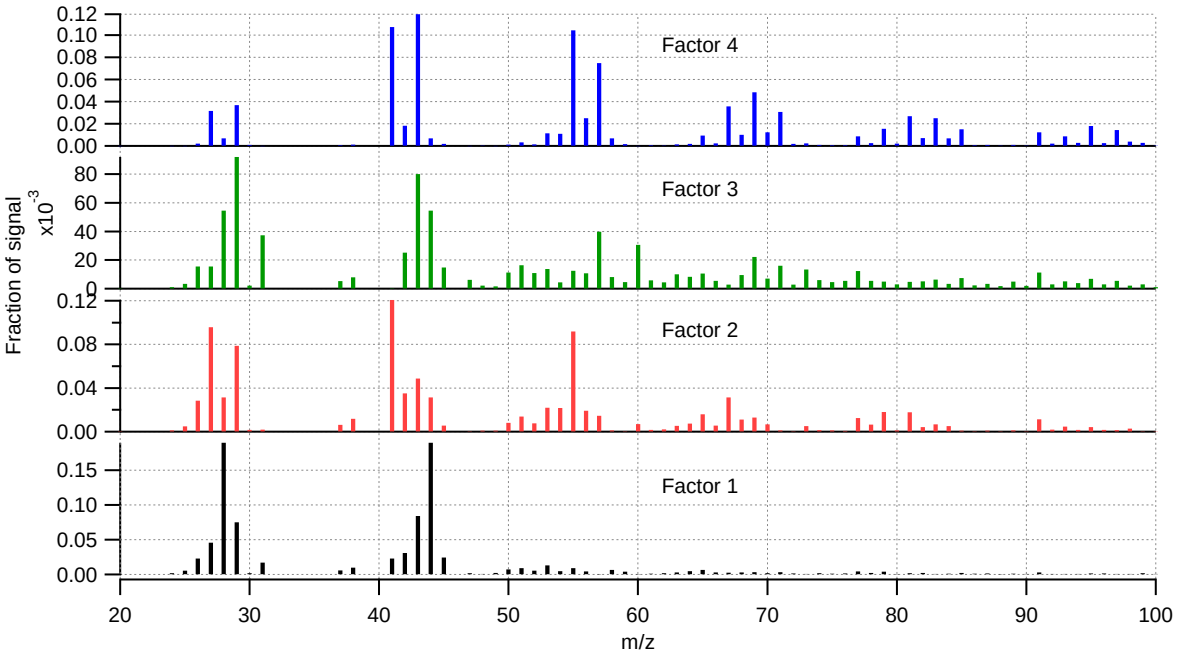

Figure S12. Mass spectra of the 4-factor solution.

4.3.2 5-factor solution

The mass spectra for the 5-factor solution (Fig. S13) are better separated compared to the 4-factor solution and the solution has a Q/Q_{exp} of 1.35003. Factor 3 from the 4-factor solution is separated in to the two different sources in the 5-factor solution. For an fPeak of 0, there is no dependence on the initialisation seed (Fig. S14).

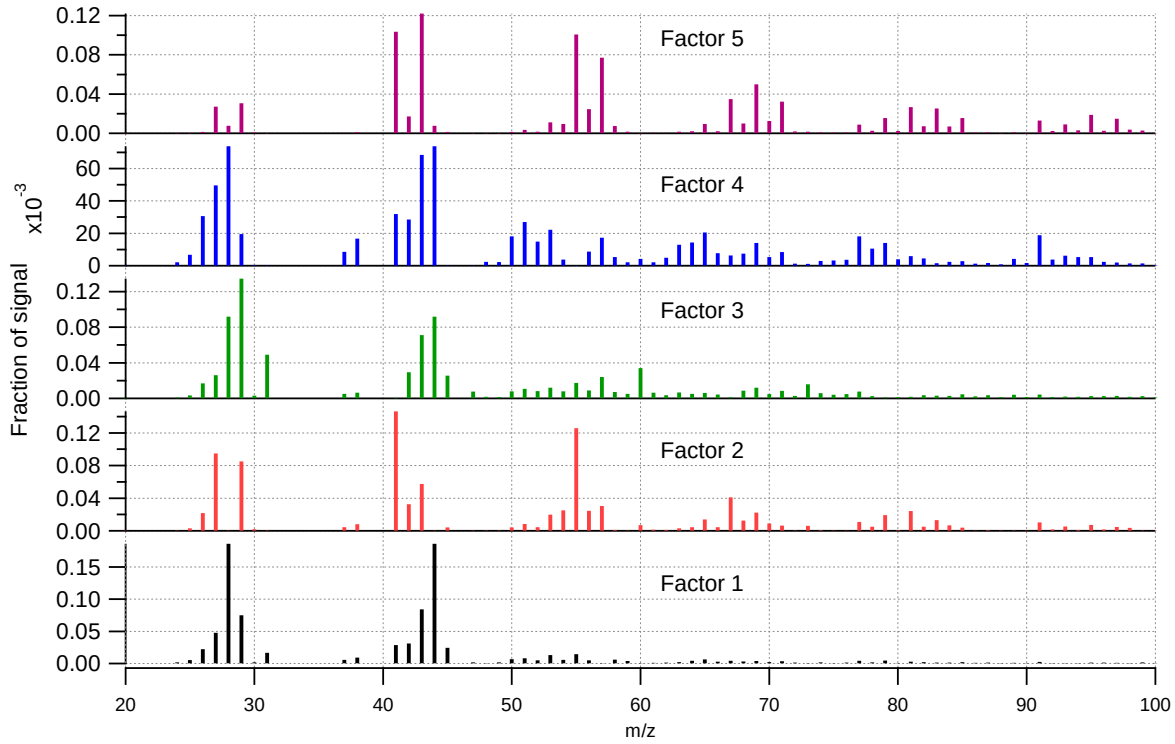

Figure S13. Mass spectra from the 5-factor solution.

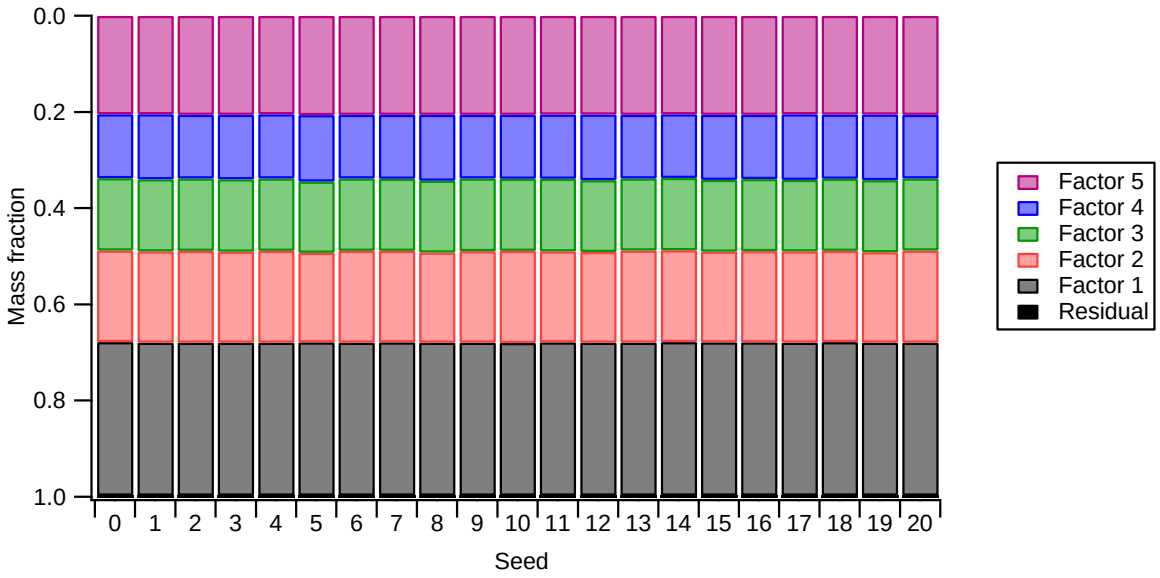

Figure S14. Variance of the factors as a function of seed from the 5-factor solution.

4.3.3 6-factor solution

Moving to the 6-factor solution, the Q/Q_{exp} decreased to 1.1433, however, the mass spectra for factors 2, 3, and 5 are similar (Fig. S15). Factors 3 and 5 exhibit alkane related peaks (e.g. at m/zs 41, 43, 55) but also additional peaks at m/zs 50, 51, 53 and 91. The time series of most of the factors co-vary in many places throughout the measurement period (sample time series shown in Fig. S16). The diurnal profiles of many of the factors are very similar, with a large peak at 21:00. This suggests that there is some mixing of the factors occurring. Furthermore, there is a little dependence on seed whereby one seed did not converge (Fig. S17). Only two fPeak values produced solutions that could be considered valid.

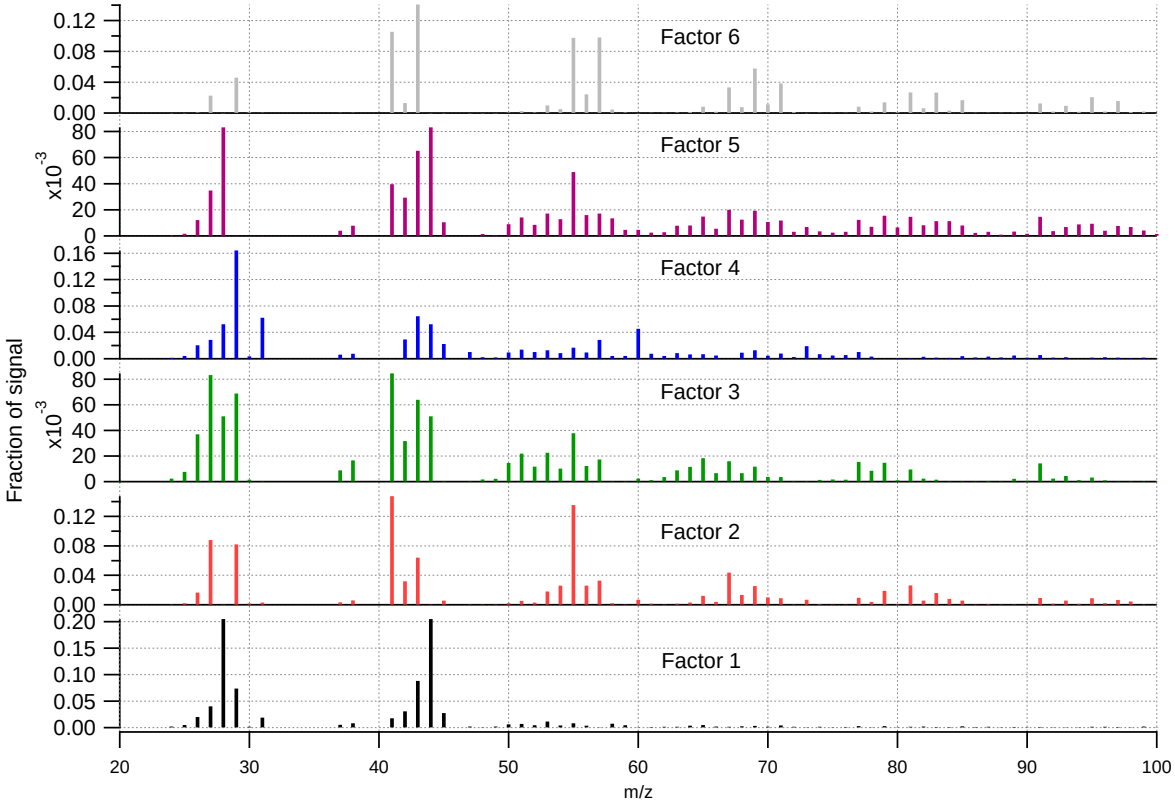

Figure S15. Mass spectra from the 6-factor solution.

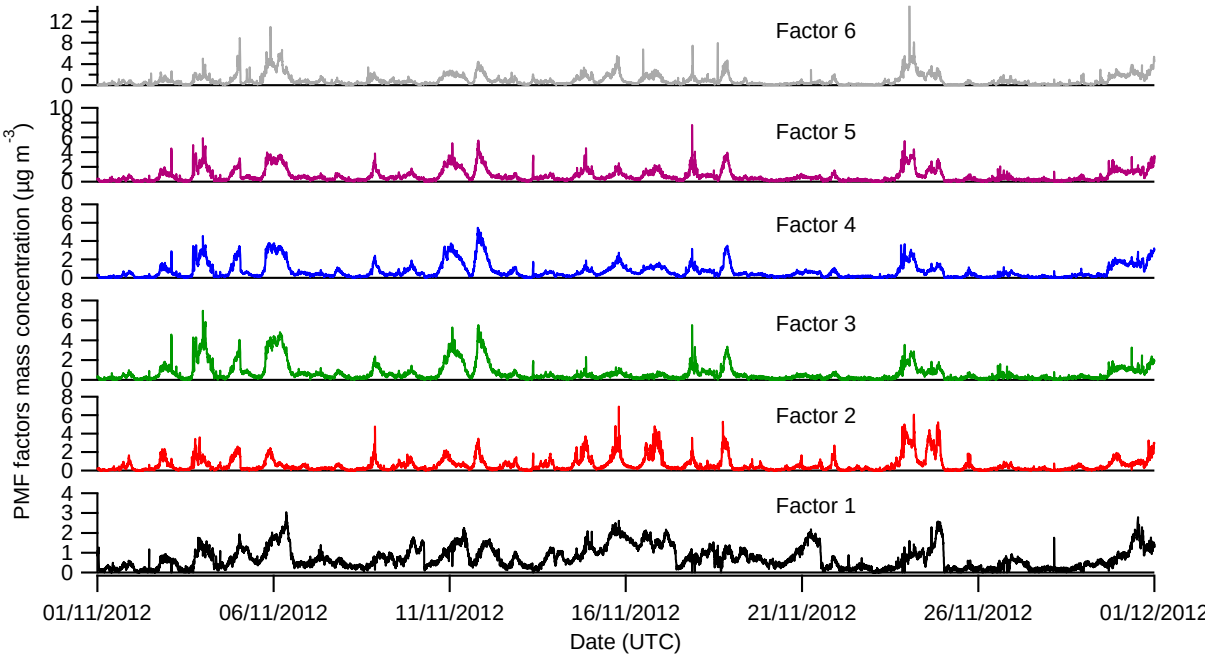

Figure S16. Sample of the time series of the 6-factor solution.

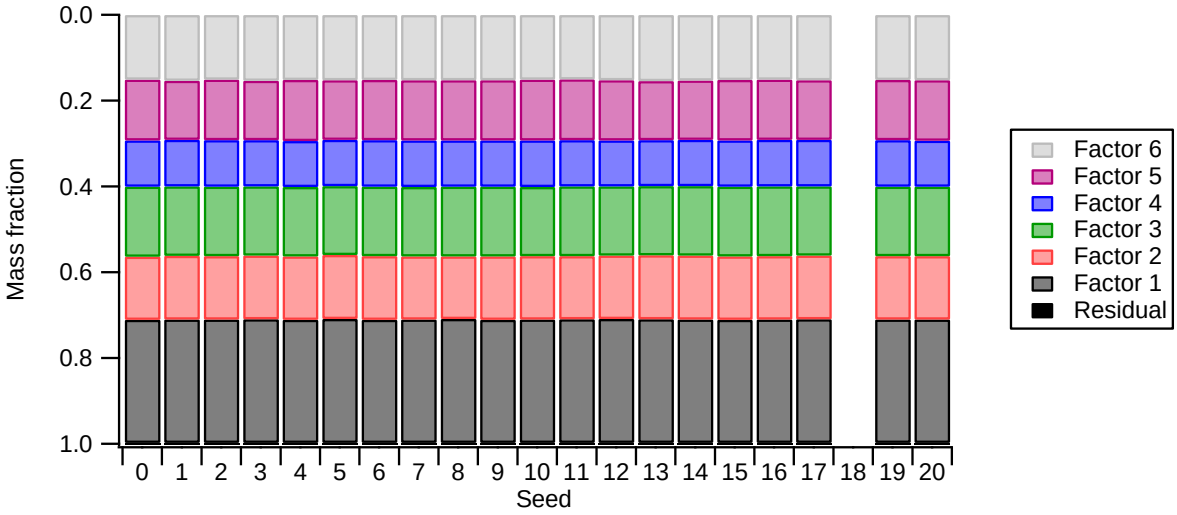

Figure S17. Variance of the factors as a function of seed from the 6-factor solution.

4.3.4 7-factor solution

The factors in this solution are even less clearly separated (Fig. S18), with factor 6 exhibiting a mass spectral profile similar to 3 and 4. Factor 1 mainly consists of peaks at m/z 28 and m/z 44 with little other signal, so is inconsistent with regular ion series. The time series of most of the factors show a similar evolution (Fig. S19), indicative of factor 'splitting'. There is also a great dependence on initialisation seed (Fig. S20) and only the solution from the most central fPeak value converged.

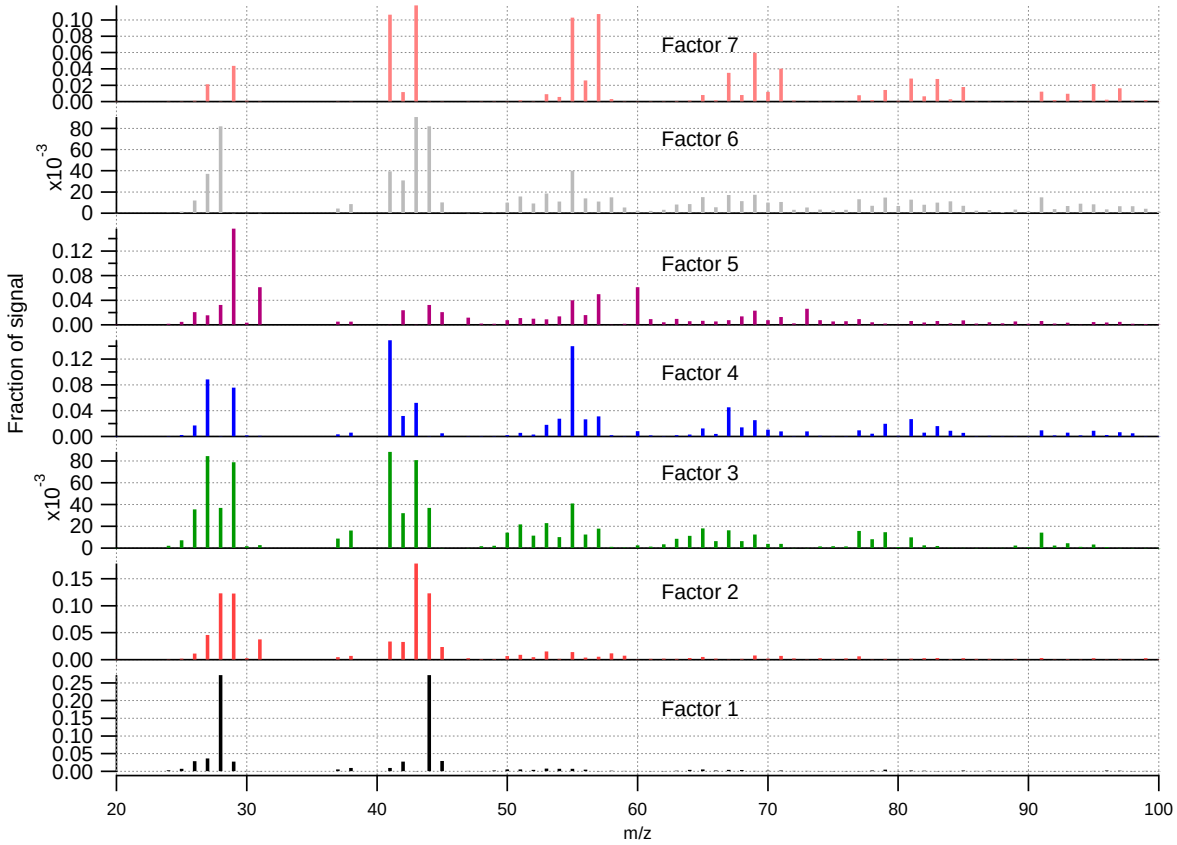

Figure S18. Mass spectra from the 7-factor solution.

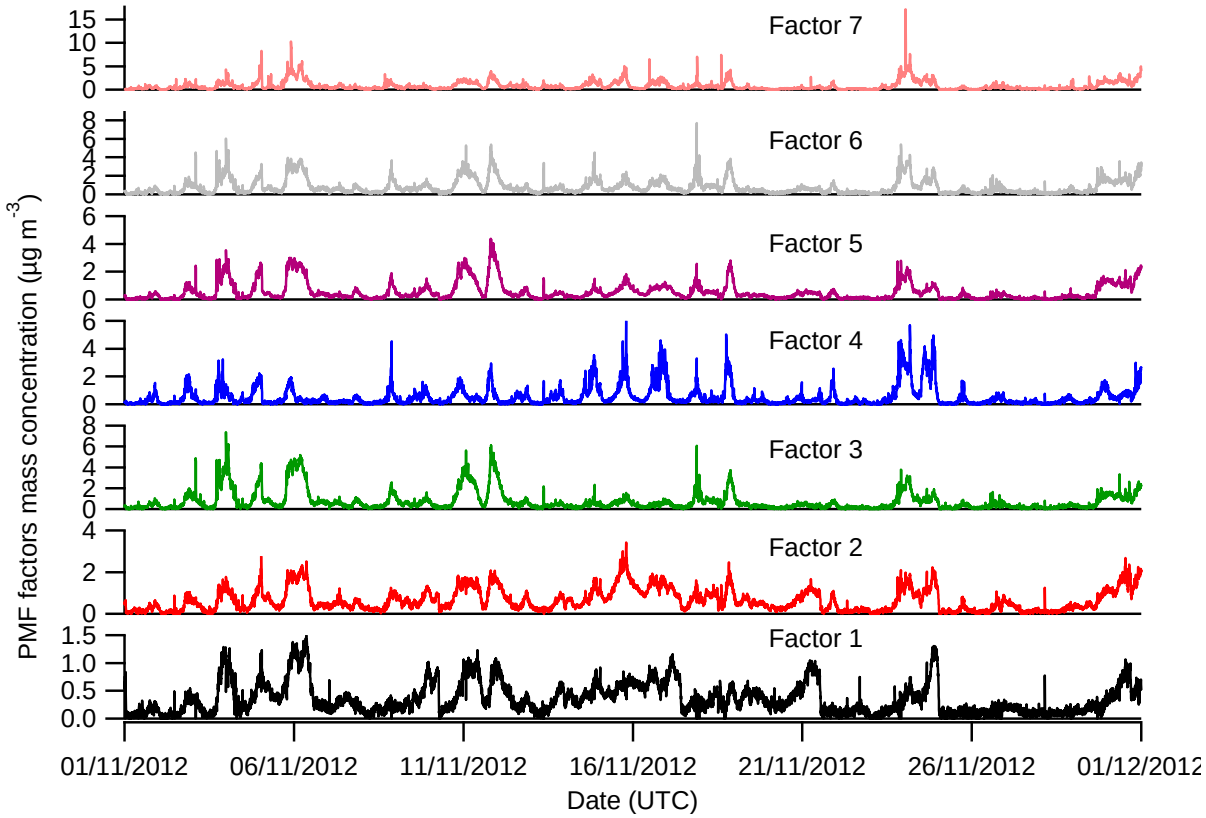

Figure S19. Sample of the time series of the 7-factor solution.

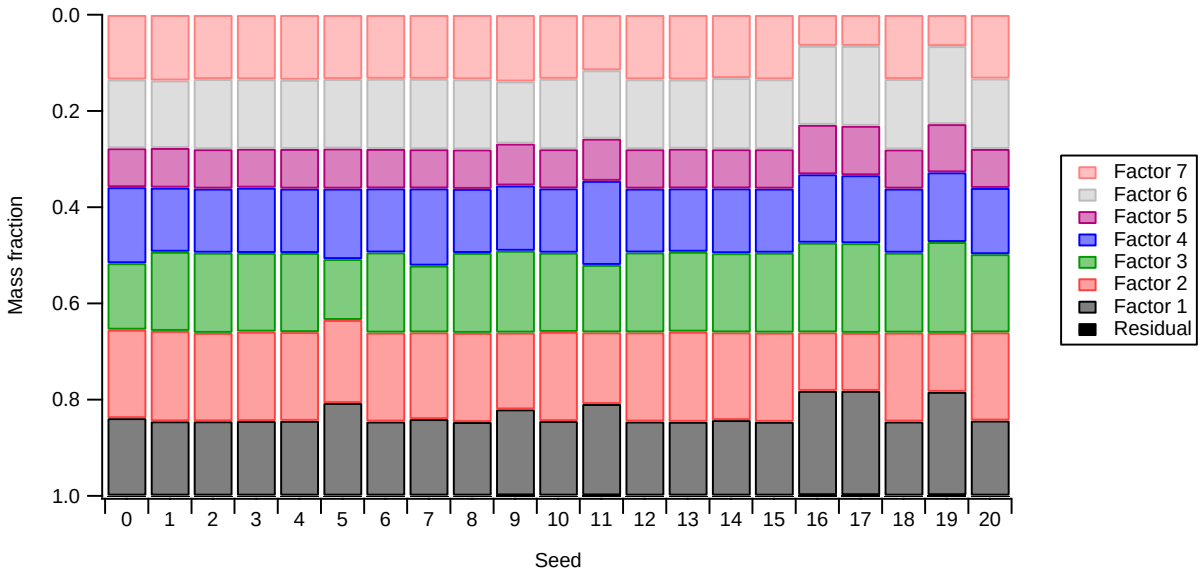

Figure S20. Variance of the factors as a function of seed from the 7-factor solution.

4.3.5 Exploring the chosen solution and identifying the factors

Table S7. Summary of the diagnostics from the different solution sets.

Number of factors (p)	Q/Qexp	fPeak values		Seed dependence?
		Convergent	Non-convergent	
4	1.44208	-1, -0.5, 0, +0.5	+1.0	No
5	1.35003	-0.6 -> +0.2 +0.6 -> +1.0	-3 -> -0.8 +0.4 +1.2 -> +3	No
6	1.26655	-0.5, 0	-1, +0.5, +1	Yes
7	1.20916	0	-1, -0.5, +0.5, +1	Yes

The 5-factor solution was chosen as it best satisfied the selection criteria (Table S7), so was further explored by running PMF with fPeak values ranging from -3 to 3 with increments of 0.2 (Fig. S21), with values between -0.6 and 0.2 as well as 0.6 and 1 producing valid solutions. Solutions from other fPeak values failed to converge.

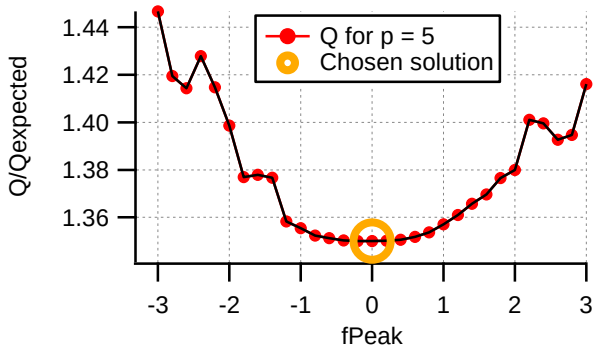

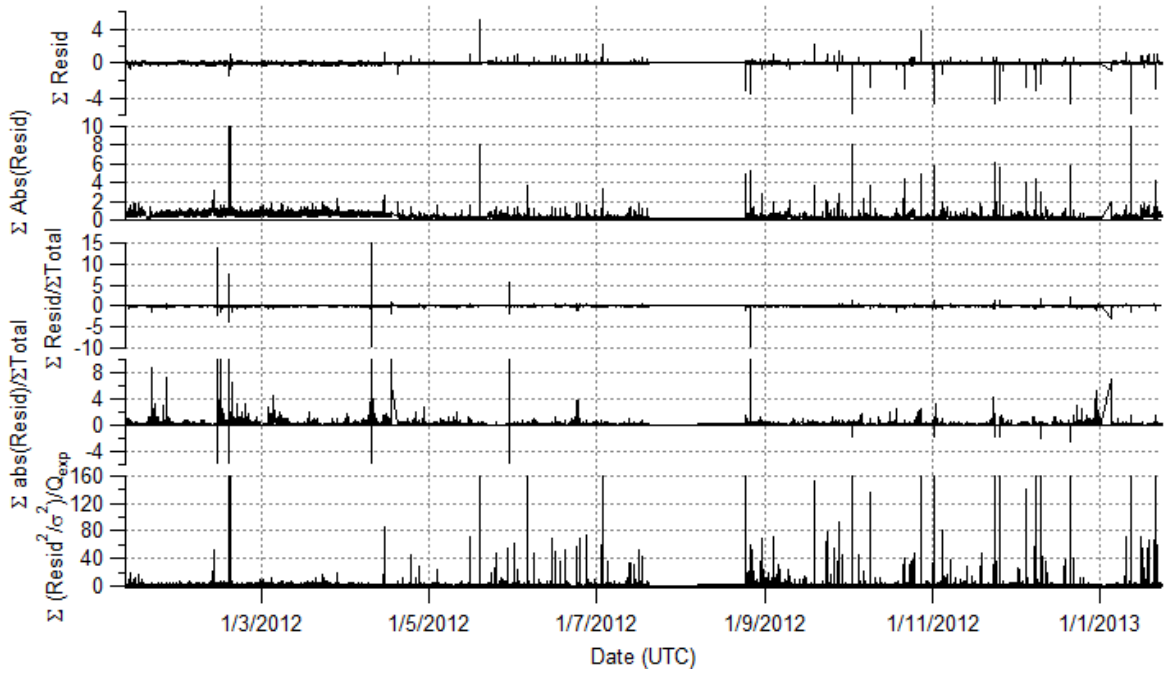

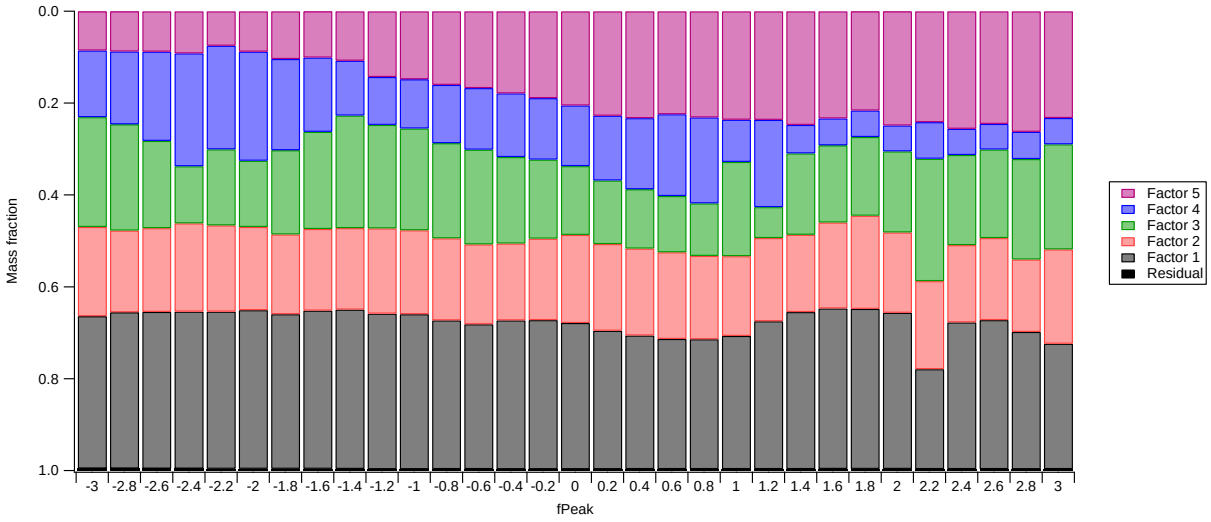

Figure S21. Top: $Q/Q_{expected}$ versus fPeak value. Middle: Time series of the residuals from PMF analysis. Bottom: Variance of the factors as a function of fPeak from the 5-factor solution.

The solutions from fPeak values -0.6 to 0.2 were investigated to further explore the rotational ambiguity of the 5-factor solution, where any changes in the concentrations of factors could be imply the amount of rotational ambiguity present in solutions (Allan et al., 2010). Here, the concentrations of factors 3 and 5, in particular, showed some variation in concentration between the different fPeak values (Table S8). However, according to Paatero et al. (2002), the solution for fPeak=0 is most likely to be physically meaningful. Therefore, this solution set is used for further analysis.

Table S8. Average mass concentration of each of the 5 factors for different fPeak values.

	Factor				
fPeak value	Factor 1 mean mass ($\mu g\ m^{-3}$)	Factor 2 mean mass ($\mu g\ m^{-3}$)	Factor 3 mean mass ($\mu g\ m^{-3}$)	Factor 4 mean mass ($\mu g\ m^{-3}$)	Factor 5 mean mass ($\mu g\ m^{-3}$)
-0.6	1.25783	0.71989	0.841235	0.557374	0.691316
0	1.2721	0.792333	0.611022	0.547316	0.845594
+0.2	1.20389	0.778428	0.564659	0.583619	0.937554

Factor 1 and factor 4 are distinct by the ratio of the m/z 44 to m/z 43 peaks, with a greater ratio for factor 1. Factors 2 and 5 were identified and separated through ordering of the peaks at m/z 41, 43, 55 and 57. In particular, the m/z 55 to m/z 57 ratio is much greater for factor 2 than for factor 5. Factor 5 was also identifiable by the peaks at m/z 41 and m/z 43 repeating every 14 mass units. Factor 3 exhibits a large peak at m/z 60, and although smaller m/z60 peaks are present in factors 2 and 4, the largest peak is in factor 3. The factors identified were hydrocarbon-like OA (HOA, factor 5), solid fuel/biomass burning OA (SFOA, factor 3), cooking OA (COA, factor 2), and the type-1 and type-2 oxygenated organic aerosols (OOA1 - factor 1 and OOA2 - factor 4, respectively).

Although there are similarities in some of the time series, it is likely that meteorological conditions and seasonal differences will result in these similarities, especially across the primary factors in the winter. For validation and increased confidence in the factorisation, the mass spectra were

compared with external mass spectral profiles (Table S9) as well as the HR-ToF-AMS profiles from the winter and summer IOPs (Section 5).

Table S9. Pearson's r correlation coefficients for comparison of the PMF factor mass spectra with reference spectra.

HOA	COA	SFOA	OOA2	OOA1
0.98	**0.86**	**0.81**	**0.83**	**0.87**
HOA	COA	BBOA	SV-OOA	LV-OOA
Reference MS	Barcelona	Reference MS	Reference MS	Reference MS
Ng et al., 2011	Mohr et al., 2012	Ng et al., 2011	Ng et al., 2011	Ng et al., 2011
0.98	**0.98**	**0.73**	**0.70**	**0.87**
HOA	COA	SFOA	OOA	OOA
Repartee 1	Repartee 1	Repartee 2	Reference MS	Reference MS
Allan et al., 2010	Allan et al., 2010	Allan et al., 2010	Ng et al., 2011	Ng et al., 2011
0.97	**0.96**	**0.94**	**0.75**	**0.98**
HOA	COA	OOA2-BBOA	OOA	OOA
Repartee 2	Repartee2	Paris	Repartee 1	Repartee 1
Allan et al., 2010	Allan et al., 2010	Crippa et al., 2013	Allan et al., 2010	Allan et al., 2010
			0.74	**0.97**
			OOA	OOA
			Repartee 2	Repartee 2
			Allan et al., 2010	Allan et al., 2010
			0.81	
			OOA2-BBOA	
			Paris	
			Crippa et al., 2013	

Furthermore, time series of additional measurements were used to validate the factors from the 5-factor solution (Fig. S22). As HOA has been found to bear a strong relationship with combustion tracers because they are emitted from car exhausts, this factor was correlated with CO and NO_x, yielding Pearson's r values of 0.66 and 0.79, respectively. The organic mass fragment at m/z 55 has been found to be an important mass fragment of COA (Lanz et al., 2007; Mohr et al., 2009; Allan et al., 2010) and is shown by the similarity of the time series of COA and org55 (0.82). SFOA correlates with org60 (0.95), a mass fragment associated with wood burning emissions (Alfarra et al 2007) and is frequently used as a tracer for SFOA/BBOA (Mohr et al., 2012; Dall'Osto et al., 2013; Crippa et al., 2013). Org60 is also associated with fatty acids from cooking POA (Mohr et al., 2009), so COA correlates relatively strongly with org60 (0.76). Relatively high correlations are shown between OOA1 and particulate sulphate and ammonium (0.71 and 0.70, respectively), similar to other urban locations (e.g. Lanz et al., 2007; Mohr et al., 2012). In contrast, OOA2 correlates only weekly with nitrate (0.28).

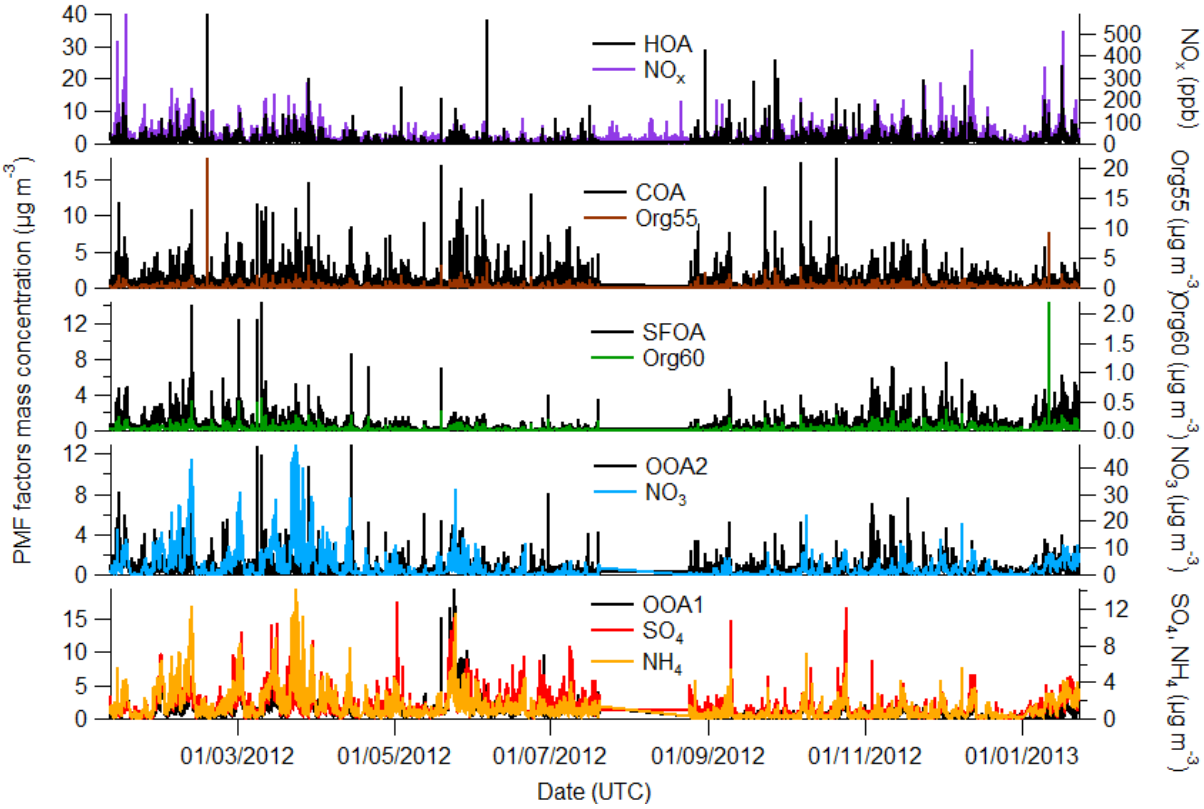

Figure S22. Time series of the 5-factor solution and ancillary data.

5 HR-ToF-AMS PMF supplementary

PMF analysis was performed on the organic data matrix from the HR-ToF-AMS from the winter and summer IOPs, where the data were pre-processed in the same way as outlined in Section 4.1.In addition, isotopes were not included in the organic matrices of the winter and summer data sets. Furthermore, the peaks at m/z 30 and 46 were removed from the organic matrices as they were not deemed to have been successfully retrieved using PIKA. The resulting matrix consisted of m/zs 12 – 115.12. APES light v1.05 (Sueper, 2008) was used for the elemental analysis of the HR-PMF factors.

The reference mass spectra used in this discussion are from the AMS spectral database. The individual spectra used are referenced appropriately. High-Resolution AMS Spectral Database. URL: http://cires.colorado.edu/jimenez-group/HRAMSsd/. Details of the databases are described in Ulbrich et al., ACP, 9, 2891-2918, 2009.

5.1 Winter IOP

5.1.1 4-factor solution

Each of the mass spectra show good separation with factor 1 being the only profile with a large peak at m/z 44 (Fig. S23). Factor 2 shows the largest peaks at m/z 60 and 73 compared to factors 1 and 2. Factors 3 and 4 can be differentiated by ordering the magnitudes of the peaks at m/z 41, 43, and 55. These factors can also be distinguished by comparing the m/z 55 to 57 ratio whereby factor 3 yields a ratio of 2.06 compared to 0.99 from factor 4. Although there are a few similarities between the

time series (Fig. S24), particularly of factors 2 and 3, real meteorological phenomena are likely influencing the mass concentrations of the aerosols emitted. The diurnal profiles (Fig. S25) exhibit unique features, such as factor 4, which has two main peaks in concentration: one at 10:00 and a broader peak in the evening with a maximum at 20:00. There was also no dependence on initialisation seed when the 4-factor solution was explored by running PMF with 50 initialisation seeds for an fPeak of 0.

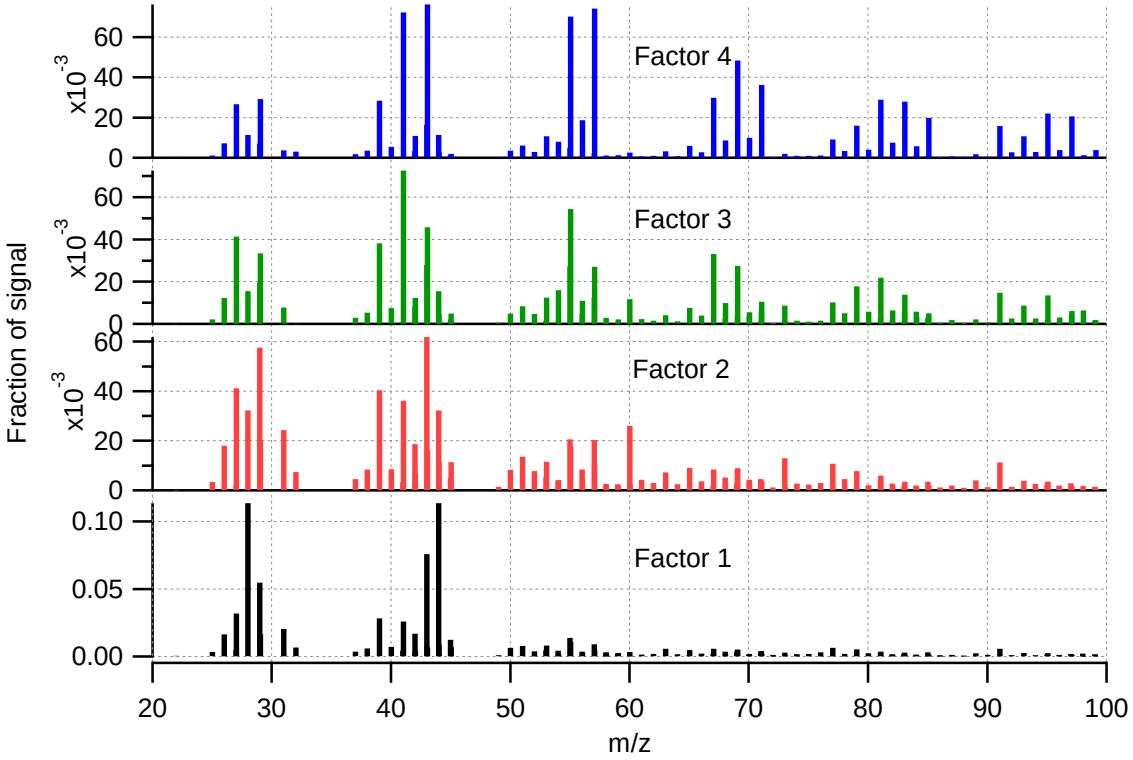

Figure S23. Mass spectra of the 4-factor solution. Note that the bars are not stacked.

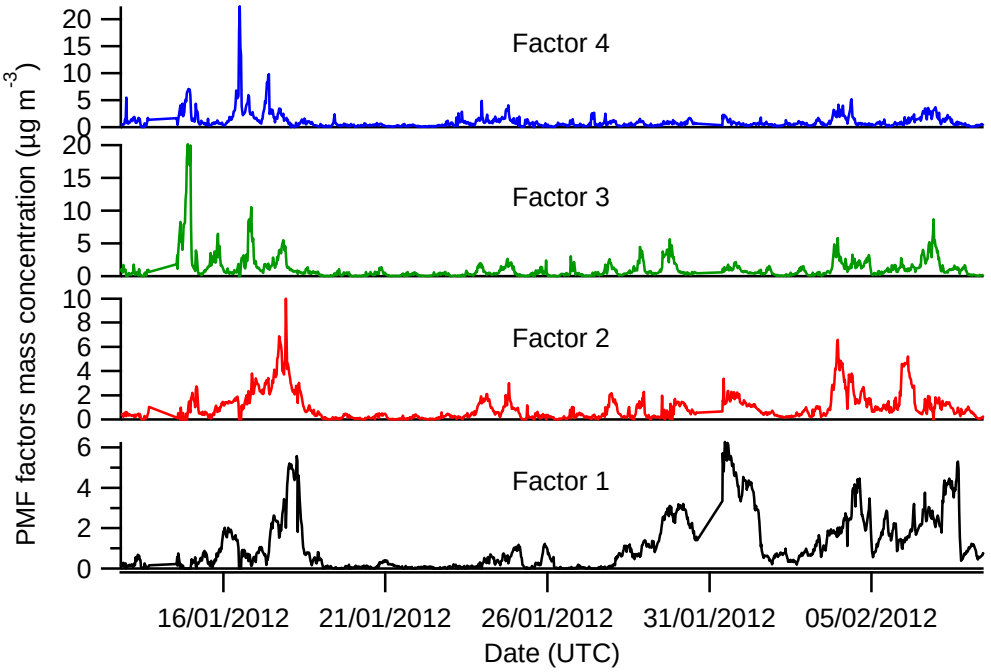

Figure S24. Time series of the factors from the 4-factor PMF solution.

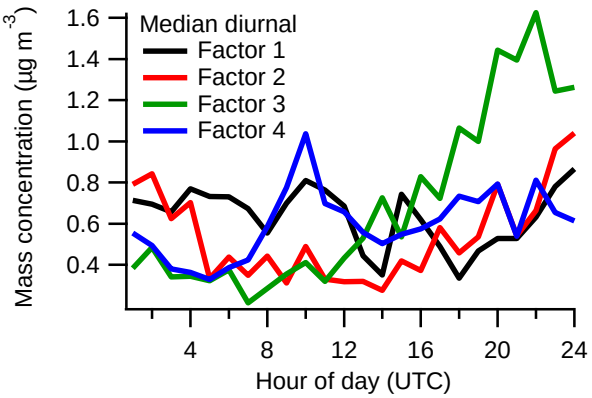

Figure S25. Median diurnal profiles of the four factors.

5.1.2 5-factor solution

Moving from the 4-factor solution to the 5-factor solution resulted in a decrease in Q/Q_{exp} to 4.375 from 4.7764. Factors 3 and 4 were found to have almost identical unit mass spectra with very similar ratios of marker m/zs such as 55/57 and 44/43, as well as similar composition (Fig. S26). However, there were some very subtle differences at m/zs 27, 29, and 41. There are also some similarities between the time series of several of the factors, particularly with factors 2 and 3 (Fig. S27). However, there are still a few differences in their time series, such as between the 4 and 6 February. It is therefore likely that factors 2 and 3 are actually a split factor, with particular events being split across the two factors.

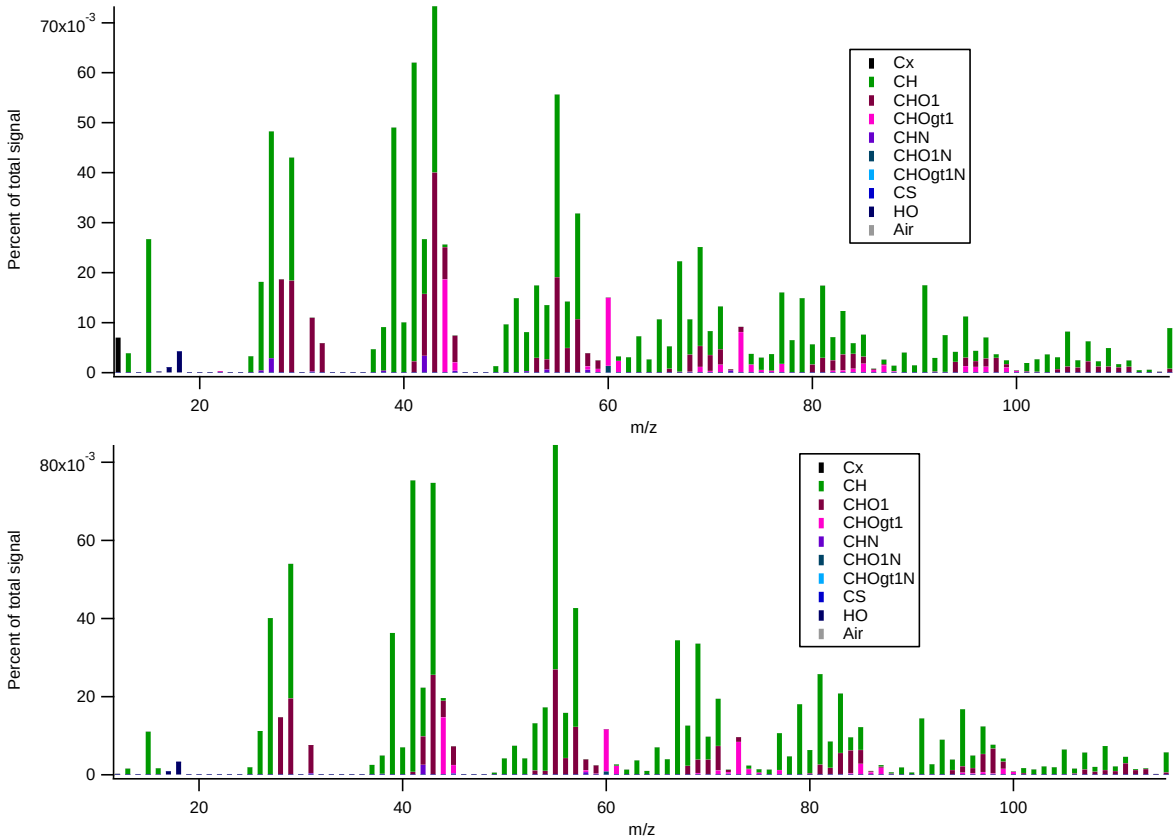

Figure S26. Mass spectra of factors 3 (top) and 4 (bottom) and their composition.

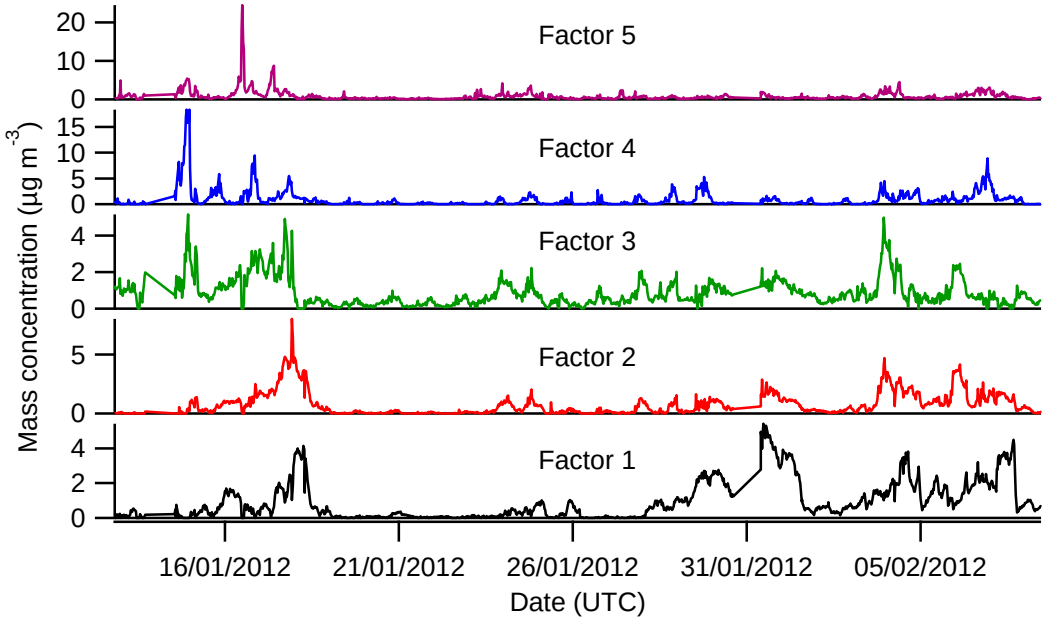

Figure S27. Time series of the factors from the 5-factor PMF solution.

This solution was explored further by running PMF with 50 seeds and it was found that there were some variations, where 2-3 different solutions were produced (Fig. S28). However, the fraction of each factor to the total does not vary significantly with seed whereby the standard deviation for each factor does not exceed 0.3% when seed 13 is excluded (Table S10).

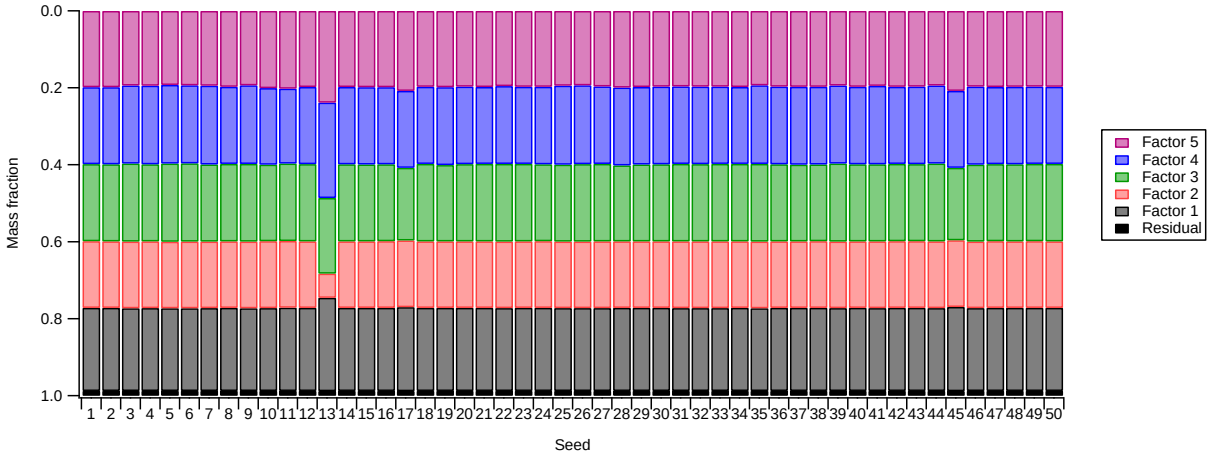

Figure. S28. Fraction of mass of each factor with change in initialisation value (seed).

Table S10. Standard deviation and percentage change of the fraction of each factor to the total mass.

	Standard deviation	%
Factor 1	0.00061147	0.061147
Factor 2	0.0001357	0.01357
Factor 3	0.00273873	0.273873
Factor 4	0.00185065	0.185065
Factor 5	0.00303816	0.303816

5.1.3 6-factor solution

The introduction of a new factor decreased Q/Q_{exp} to 4.1248 however, the solution set did not converge at fPeak=0. The lowest Q/Q_{exp} was obtained with an fPeak=-0.5, which resulted in the profiles in Fig. S29, where factor 1 consists mainly of a signal at m/z 32 and results in a noisy time series (Fig. S30) and the other mass spectra and times series appear very similar to the 5-factor solution.

There was also a significant dependence on the initialisation seed used, which produced two general types of solution, of which only one converged. Due to this considerable dependency on seed and unrealistic factor, this solution set was discarded.

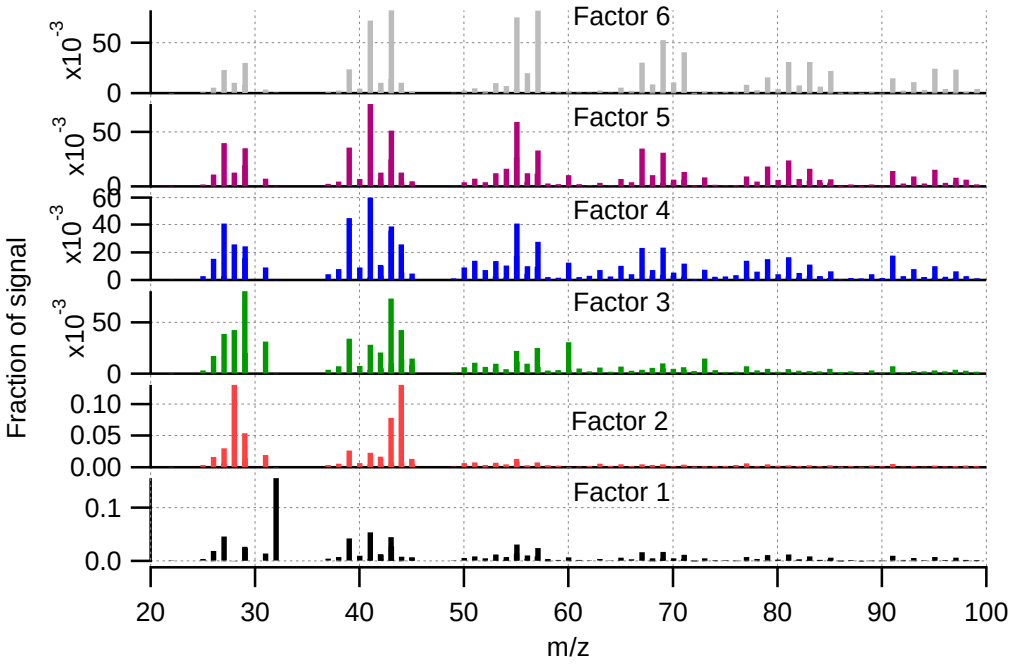

Figure S29. Mass spectra of the 6-factor solution. Note that the bars are not stacked.

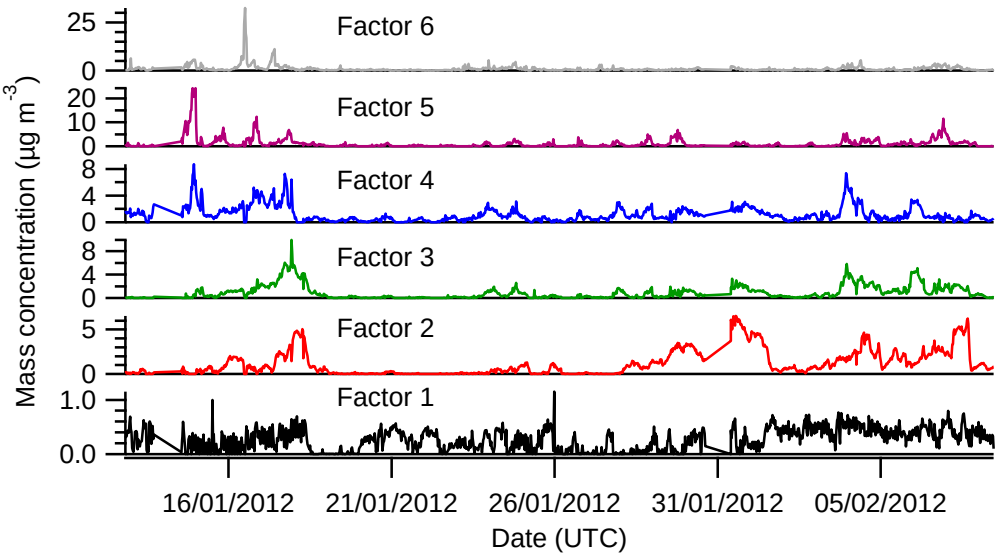

Figure S30. Time series of the 6-factor solution.

5.1.4 Exploring the 4 and 5-factor solutions

The factors for the 4-factor solution are identified as OOA, SFOA, COA, and HOA. The interpretation of each of the factor sources is supported by the comparison of both reference mass spectra and time series from other independent measurements taken at the North Kensington site.

For the mass spectra, factor 1 compares with the LV-OOA and SV-OOA reference spectra from Mohr et al. (2012) with Pearson's r values of 0.95 and 0.85, respectively, and also with the unit mass OOA from Ng et al. (2011) with an r of 0.82. The time series of this factor correlates with ambient HR-ToF-AMS data such as nitrate, sulphate, and ammonium with Pearson's r of 0.87, 0.85, and 0.91, respectively, which is consistent with other urban locations (Lanz et al., 2007; Crippa et al., 2013).

Comparison of factor 2 with the standard BBOA spectrum from Ng et al. (2011) yields a Pearson's r value of 0.96. The peaks at m/z 60 and 73 are smaller than those at m/z 29, 43, and 44 in factor 2. However, as peaks at m/z 29, 43, and 44 are found in most PMF mass spectra they cannot be used as a tracer for SFOA (Alfarra et al., 2007). Nevertheless, the correlation between the time series of SFOA and org60 yields a Pearson's r of 0.86. The mass increases from approximately 15:00 and peaks overnight, decreasing to the average daytime mass at 5:00. The greater mass at night compared to during the day is expected from evening activities in the house, where space heating is used during the winter months.

Factor 3 shows a strong correlation with the COA spectral profiles from Mohr et al (2012), with a Pearson's r of 0.88. Similarly when compared to ancillary data, factor 3 has a strong relationship with org55 (r=0.85). A large evening peak is observed in the diurnal cycle, which starts to increase from about 12:00, reaching a peak at 21:00 and rapidly decreasing. The large evening peak is likely associated with local residents cooking meals. In addition, this could be due to the cooking activities from the numerous restaurants on Portebello Road, which is approximately about 350 m from the site. The restaurants are likely to open for lunchtime, which could explain why the increase in mass occurs at this time.

A Pearson's r value of 0.99 is obtained when factor 4 is correlated with the HOA mass spectral profiles from Mohr et al. (2012) and Ng et al. (2011). OA has been found to show bear a strong relationship with combustion tracers because they are emitted from car exhausts, so factor 4 was correlated with the BC equivalent mass from the aethalometer (880 nm), CO, and NO_x and yielded Pearson's r values of 0.68, 0.64, and 0.69, respectively. However, the strongest correlation was found when the time series of factor 4 was correlated with org57 (r=0.87). This factor exhibits a diurnal pattern with a large peak at 9:00 and a smaller, broader peak in the evening, which correspond to rush-hour activity.

For the 5-factor solution, the factors were identified as OOA, SFOA1, SFOA2, COA, and HOA. Comparison of the factors with ancillary data (Fig. S31) supports the attribution of the factors, with Pearson's r values for ammonium, nitrate, and sulphate with respect to OOA of 0.90, 0.86, and 0.86, respectively. There is a strong correlation between the time series of COA and org55 (r=0.83). org57 has also been found to be a tracer for HOA (Zhang et al., 2005) and is found to strongly correlate with the time series of HOA (r=0.81). Factors 2 and 3 correlate with org60 (r=0.85 and 0.79 respectively). Furthermore, the time series of the factors correlated well with black carbon measurements (Liu et al., 2014) and CMB outputs (Yin et al., 2014).

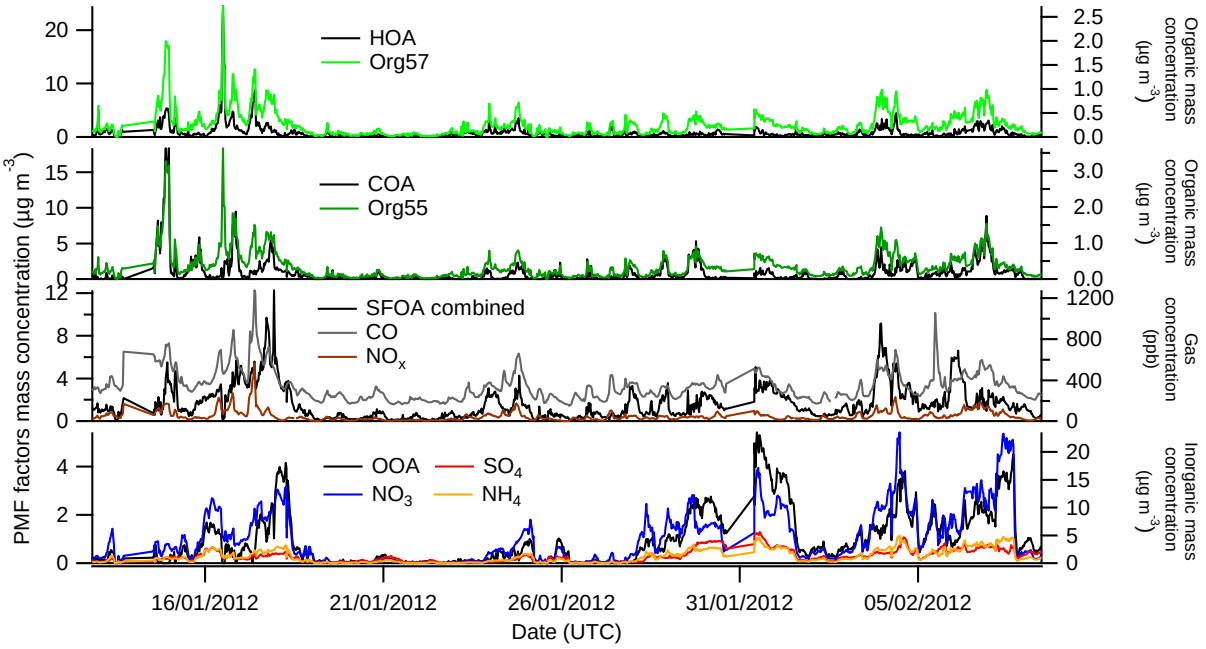

Figure S31. Time series of each PMF factor and time series of ancillary data. All data are measured by the AMS apart from CO and NO_x, which have been provided by James Lee.

Based on the similarities of the time series, diurnal cycles, and correlation with ancillary data factors 2 and 3 have been regrouped to one SFOA using the sum of their time series. Comparison of the time series from the combined SFOA factor and the remaining factors from the 5-factor solution with the corresponding factors from the 4-factors solution highlights some differences (Fig. S32). However, the factors from the two different solution spaces correlate very well (Table S11). With the exception of a few events where the mass of the 5-factor solution is less than that of the 4-factor solution, there is little difference between the HOA and COA factors between the two solution sets. For SFOA, the combined factor has a greater mass than that of the 4-factor solution, with the converse being true for the OOA factor.

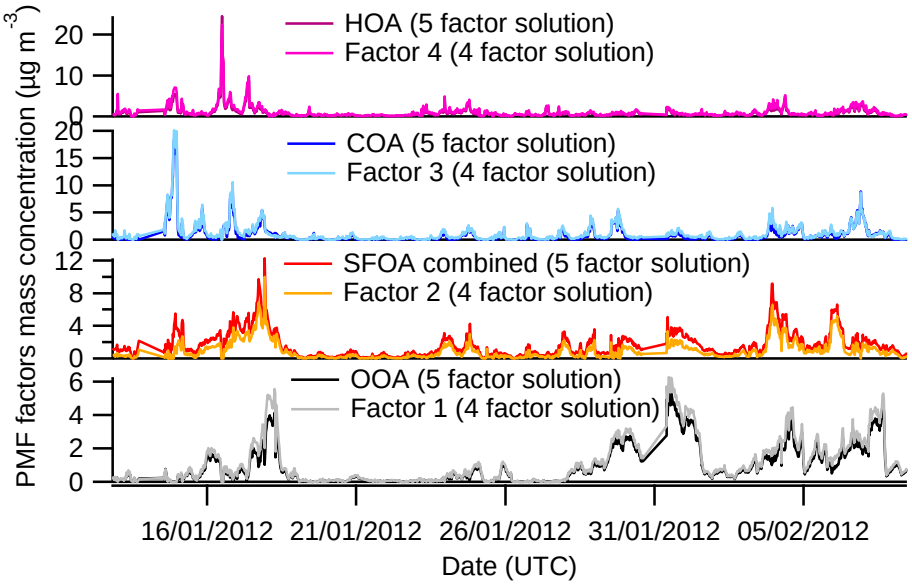

Figure S32. Comparison of the time series of the 4-factor solution and 5-factor solution with two factors combined.

Table S11. Pearson's r value (and slope) for each of the factor correlations.

	4-factor solution			
5-factor solution	HOA	COA	SFOA	OOA
HOA	0.99 (0.93)			
COA		0.99 (0.92)		
Combined SFOA			0.98 (1.34)	
OOA				1.00 (0.83)

The diurnal cycle of the combined factor clearly exhibits an increased concentration overnight (Fig. S33), which is consistent with the expected use of space heating in the evenings during winter.

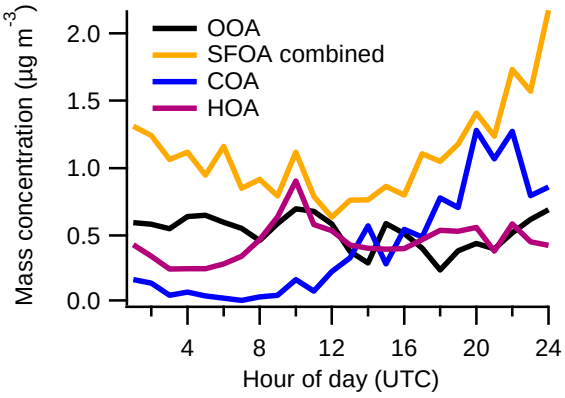

Figure S33. Diurnal cycle of the four factors from the 5-factor solution where the two SFOA factors have been combined.

It has been shown that NO_x and CO are strongly related to HOA (Zhang et al., 2005) as they are emitted from fuel combustion in vehicle engines. However, traffic activity is not the only source of these gases, which are used as tracers for combustion. Space heating has been found to be another

potential combustion source and therefore contributes to SFOA (Allan et al., 2010). The Pearson's r values derived between the gas tracers and the SFOA factor from the 4-factor solution (hereon in termed SFOA-4fac) are shown in Table S12. When the two SFOA factors from the 5-factor solution (SFOA-combined) are summed and compared to the gas tracers the Pearson's r values are better than those for SFOA-4fac. However, as both traffic and domestic fuel burning from space heating contribute to CO and NO_x concentrations a multi-linear regression fit as detailed in Allan et al. (2010) was performed to assess the relative contributions of traffic (HOA) and wood burning (SFOA) to these trace gases.

Fitting was performed according to the function:

$$f\,(\mathrm{HOA, SFOA}) = A[\mathrm{HOA}] + B[\mathrm{SFOA}] + C$$

where [HOA] and [SFOA] are the concentrations of the HOA and SFOA PMF factors and *A*, *B*, and *C* are arbitrary fitting parameters optimised to minimise the squared difference between *f* (HOA, SFOA) and NO_x or CO. This multi-linear regression fit was performed on the HOA and SFOA factors from the 4-factor solution and the HOA and combined SFOA factors from the 5-factor solution. The Pearson's r values derived are shown in Table S12. Including both sources in this way significantly improves the correlations with the gas tracers for both sets of solutions. However, there is little difference between the regression fit r values for the two solution sets with the 4-factor solution showing a very slightly greater correlation with NO_x than the 5-factor solution.

Table S12. Pearson's r correlation coefficients for linear and multi-linear regressions between PMF factors from the 4 and 5-factor solutions and combustion tracers.

	CO	NO_x
SFOA-4fac	0.56	0.43
SFOA-combined	0.65	0.51
f(HOA,SFOA)-4fac	0.77	0.74
f(HOA,SFOA)-combined	0.77	0.71

Ultimately, there is little difference between the SFOA derived in the 4-factor solution to the combined factor from the 5-factor solution and so both could be valid solution sets. However, because the 5-factor solution with the two SFOA factors combined has a lower Q/Q_{exp} than the 4-factor solution this is the solution set that is used in further analyses. In summary, four main components were identified: oxygenated OA (OOA), solid fuel OA (SFOA), cooking OA (COA), and hydrocarbon-like OA (HOA) where the two SFOA factors from the 5-factor solution were combined.

Finally, rotational ambiguity within the 5-factor solution was explored through the fPeak value where values between -0.6 and 1.0 produced solutions that could be considered valid and outside of this range, solutions produced nonphysical factors or failed to converge properly (Fig. S34). Between these values, however, the concentrations of HOA and COA showed some variation (Table S13) although the ambiguity was not a direct rotation between these two factors as the HOA profile was consistent between all fPeak values. Instead, the exchange of signals between profiles seemed to involve the COA and two SFOA factors. However, as the solution for fpeak=0 is most likely to be physically meaningful according to Paatero et al. (2002), this most central solution is used for further

analysis. Furthermore, this solution space was found to be relatively stable, produced good separation of the factors and the lowest $Q/Q_{expected}$.

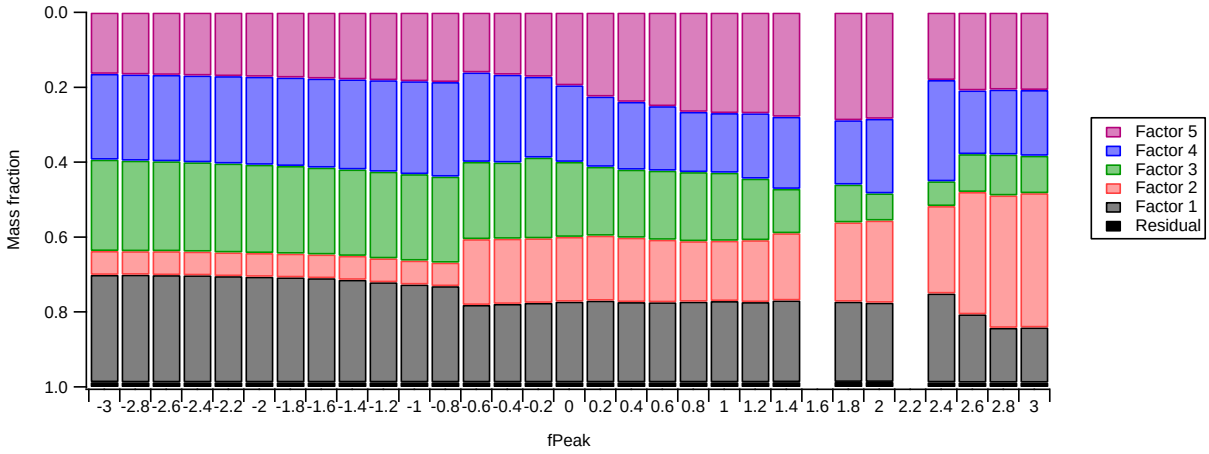

Figure S34. Variance of the factors as a function of fPeak from the 5-factor solution.

Table S13. Average mass concentration of each of the 5 factors for different fPeak values.

	Factor				
fPeak value	OOA	SFOA1	SFOA2	COA	HOA
-0.6	0.897374	0.757835	0.882626	1.02376	0.68164
0	0.933063	0.747544	0.857564	0.875335	0.829156
1	0.940803	0.696752	0.776001	0.682512	1.14724

5.2 Summer IOP – data in UTC (BST +1)

5.2.1 4-factor solution

There is a clear separation of the mass spectra for the 4-factor solution (Fig. S35) where the different factors are identified by their characteristics peaks. For example, although factors 1 and 2 exhibit very similar mass spectra they differ in m/z 44/43 ratio, with factor 1 having a larger m/z 44 peak indicative of a greater degree of oxidation, where this peak is associated with the CO_2^+ ion. Factors 3 and 4 differ in the ordering of the magnitudes of the peaks at m/z 41, 43, 55, 57. The time series of the factors are also distinct from each other (Fig. S36).

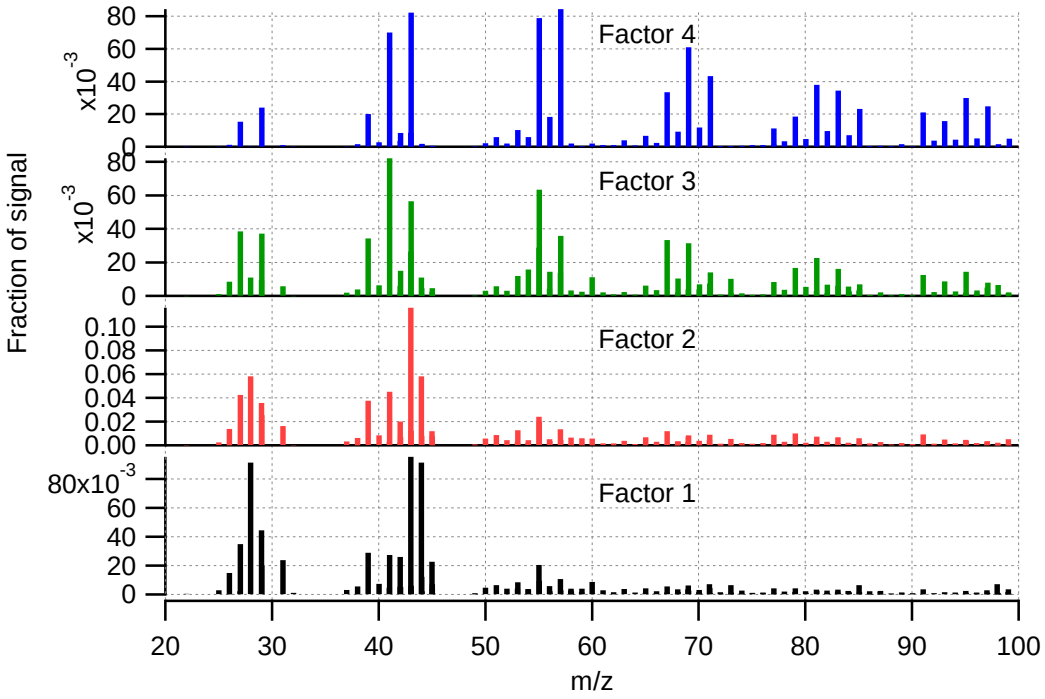

Figure S35. Mass spectra of the 4-factor solution. Note that the bars are not stacked.

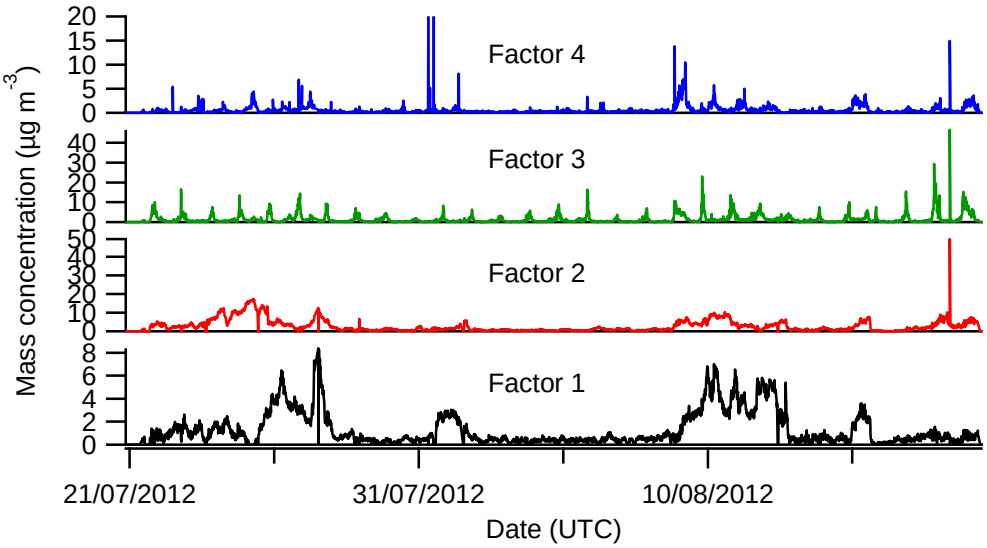

Figure S36. Time series of the 4-factor solution.

When this solution space was explored by running PMF with 50 seeds, some dependency was observed (Fig. S37). Although there was very little variation in the fraction of each factor with seed, there were some changes in fractional contribution between factor 1 and factor 2. This suggests some rotation between these two factors whereby both factors exhibit a larger m/z 43 peak than m/z 44. For these reasons, a 5-factor solution was explored.

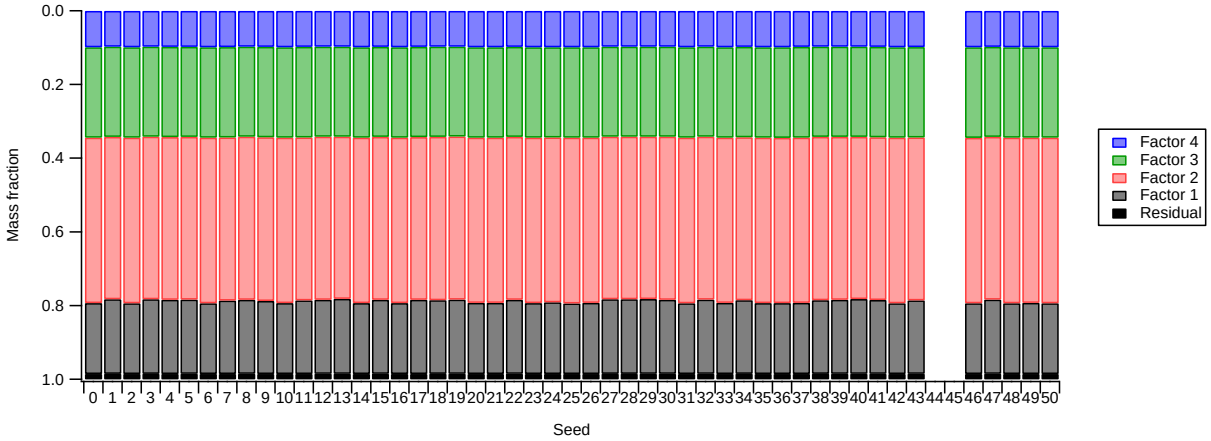

Figure S37. Fraction of mass of each factor with change in initialisation seed.

5.2.2 5-factor solution

Moving to a 5-factor solution the Q/Q_{exp} decreases to 2.4408 and there is still relatively good separation between the mass spectra (Fig. S38), each with a unique time series (Fig. S39) and diurnal profile (Fig. S40). Furthermore, there was no dependence on initialisation seed (Fig. S41). Factors 1 and 2 are better defined than in the 4-factor solution as factor 1 has a larger peak at m/z 44 than m/z 43, whereas the converse is true for factor 2. Factors 2, 4, and 5 are very similar to factors 2, 3, and 4 in the 4-factor solution. The new factor, factor 3, features similar peaks to factors 2 and 4, with a particularly large peak at m/z 43. The diurnal profile exhibits a unique increase in mass from around 21:00 and decreases late in the morning. No other profiles show this overnight peak.

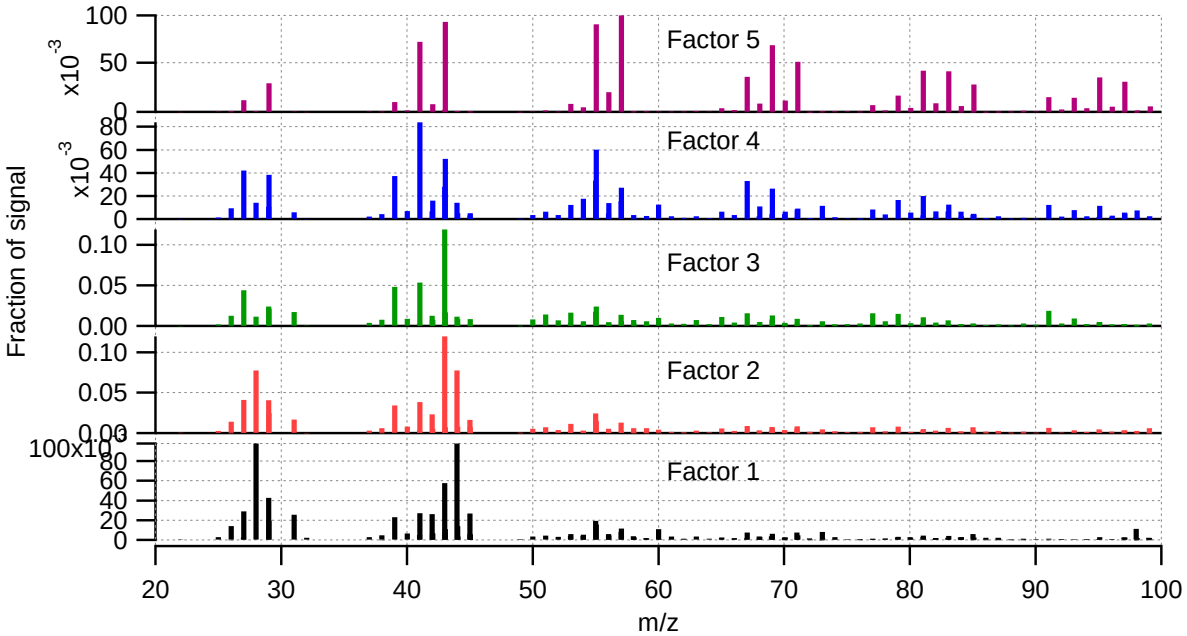

Figure S38. Mass spectra of the 5-factor solution. Note that the bars are not stacked.

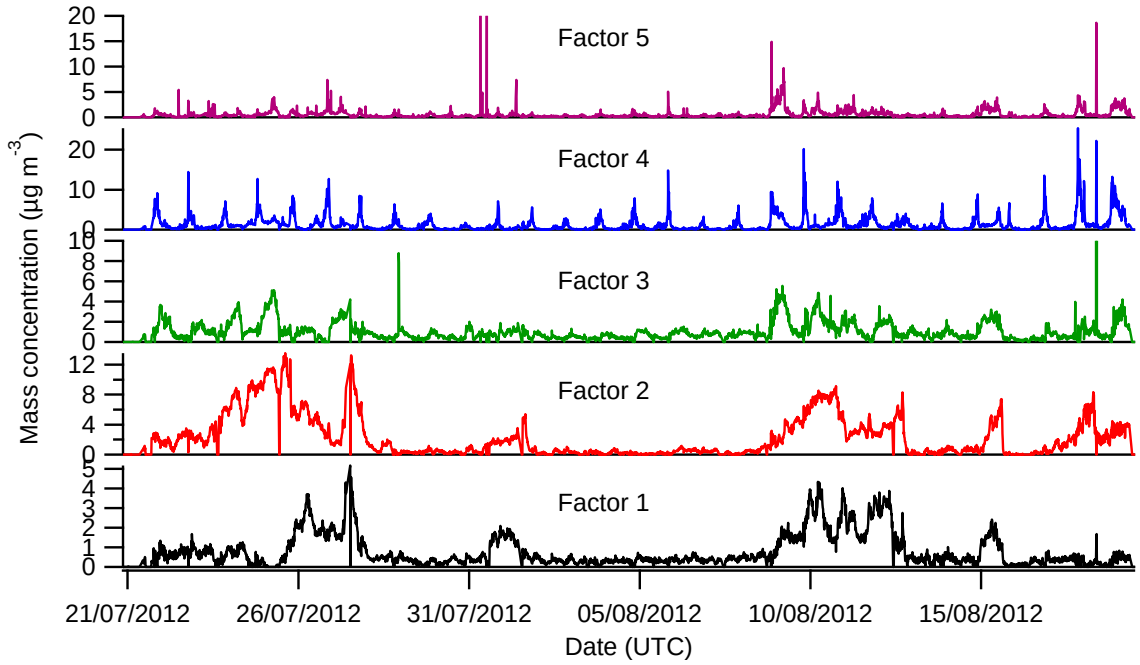

Figure S39. Time series of the 5-factor solution.

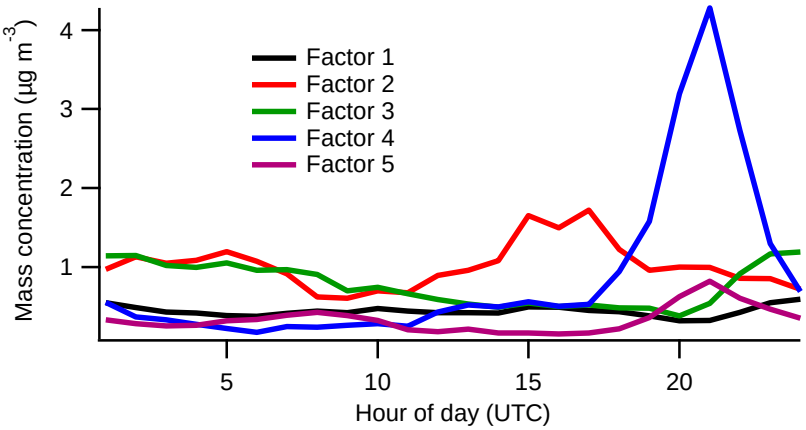

Figure S40. Median diurnal profiles of the 5 factors.

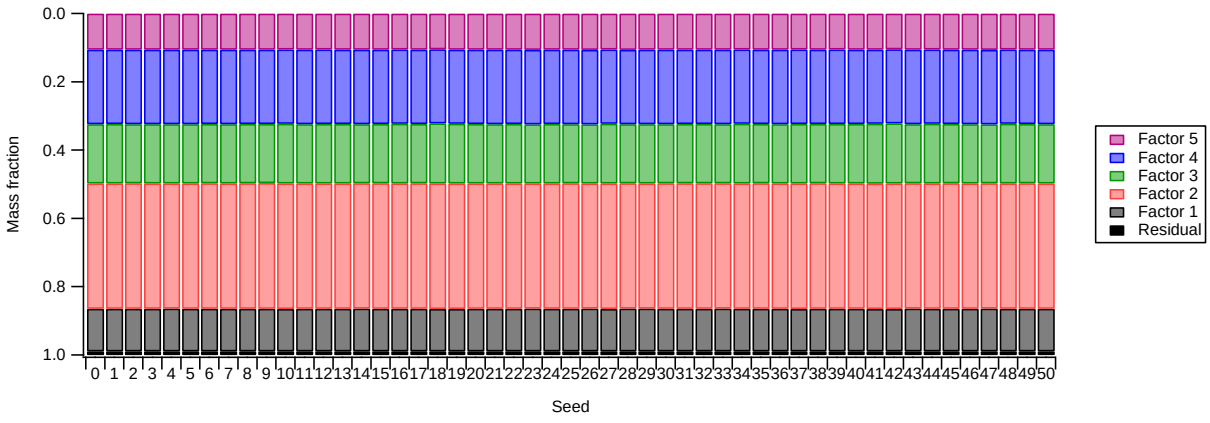

Figure S41. Fraction of mass of each factor with change in initialisation seed.

5.2.3 6-factor solution

Moving to a 6-factor solution the Q/Q_{exp} decreases to 2.272 from 2.4408, however the new factor, factor 4, consists mainly of a large peak at m/z 43 (Fig. S42). There are similarities in the time series between factors, with factor 4 showing similar trends to factors 1 and 3 (Fig. S43) as well as a very similar diurnal pattern to factor 1 (Fig. S44).

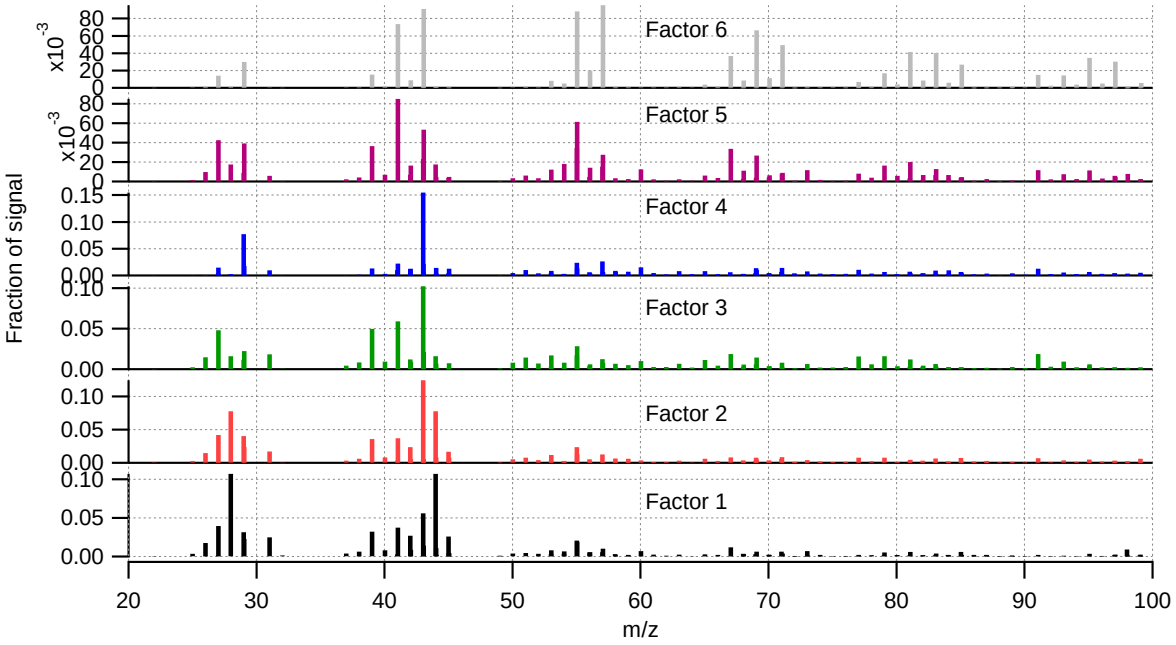

Figure S42. Mass spectra of the 6-factor solution. Note that the bars are not stacked.

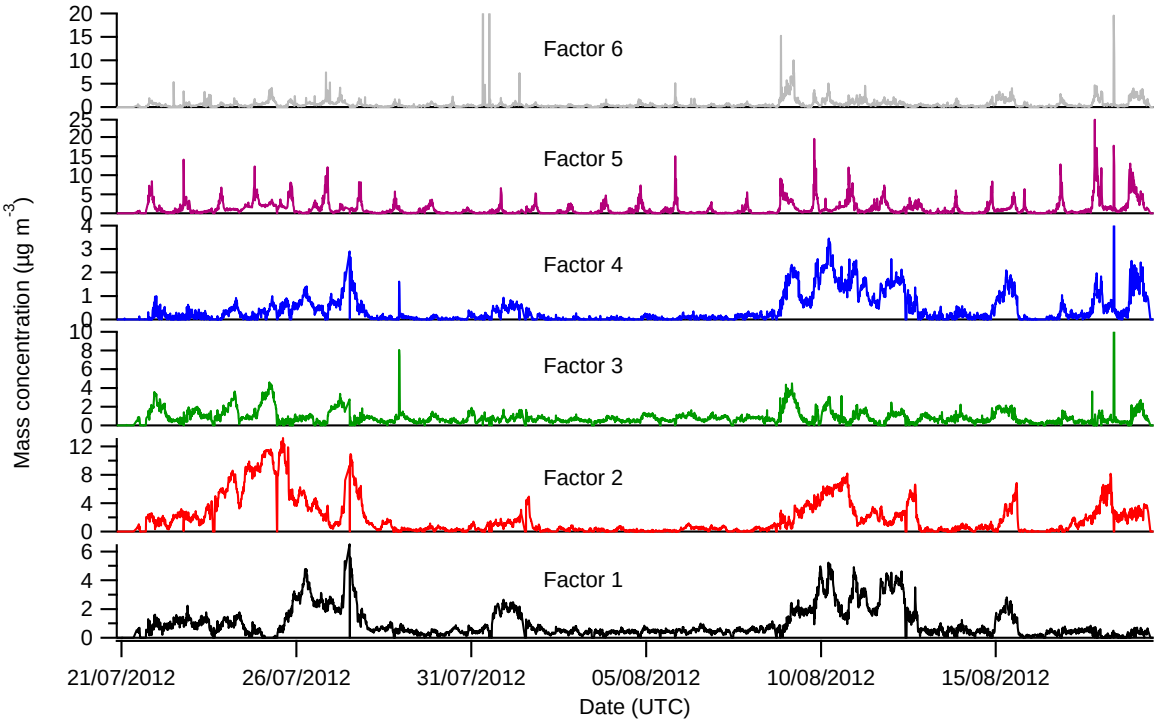

Figure S43. Time series of the 6-factor solution.

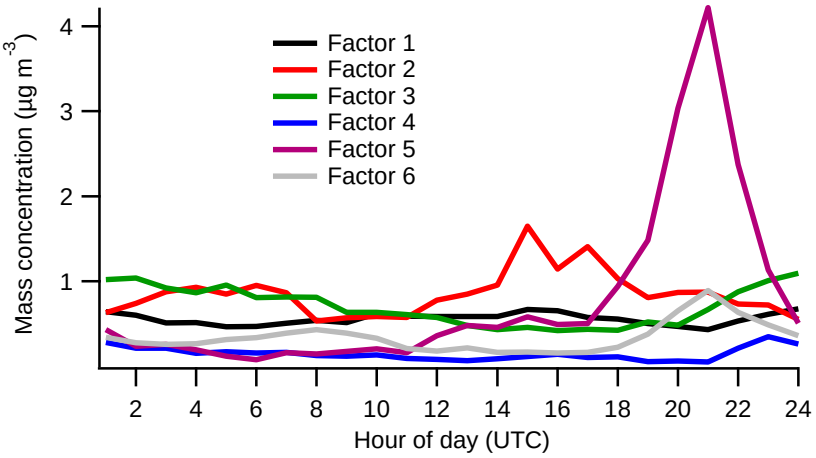

Figure S44. Median diurnal profiles of the 6 factors.

However, there are some subtle differences compared to the factors from the 5-factor solution including an increased m/z 57 to 55 ratio for factor 5 compared to factor 4 in the 5-factor solution. There are also several similarities in their time series as shown in Figure S45.

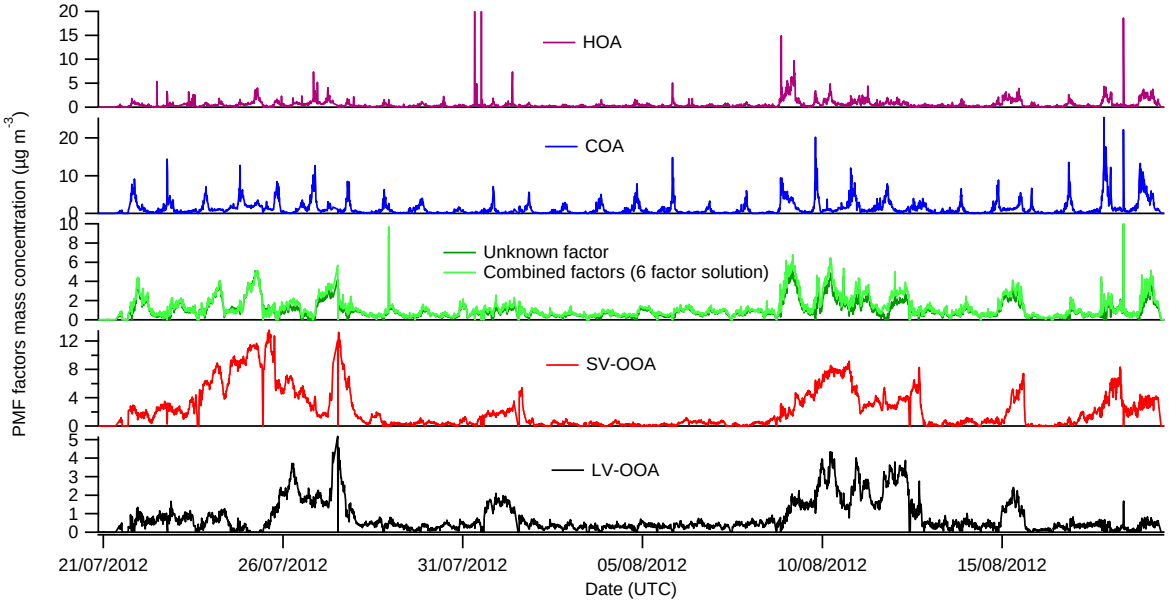

Figure S45. Time series of the 5-factor solution with factors 3 and 4 from the 6-factor solution combined, where factor 3 in the 5-factor solution is in dark green and the light green trace is factors 3 and 4 from the 6-factor solution summed.

There is negligible difference between the combined factor from the 6-factor solution and the unknown factor from the 5-factor solution, yielding an r of 0.97 when correlated. These similarities in time series and mass spectra are indicative of factor splitting. Furthermore, the 6-factor solution showed considerable dependency on initialisation seed used, whereby two main solutions result from the different seeds (Fig. S46). There is variance within each of these solution groups and one group of solutions does not converge. The 6-factor solution is therefore not stable and was discarded.

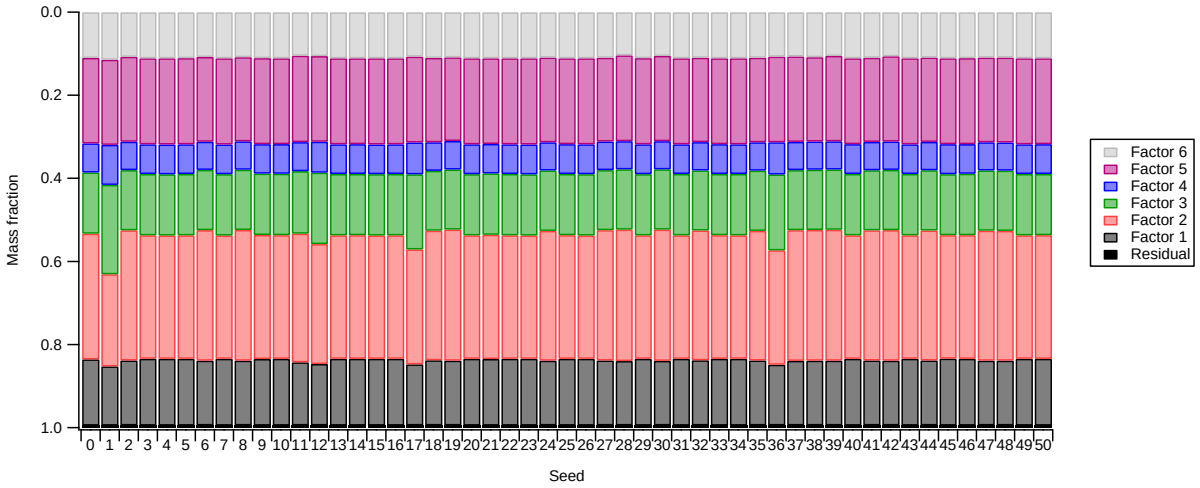

Figure S46. Fraction of mass of each factor with change in initialisation seed.

5.2.4 Factor identification and interpretation of the chosen solution set

In order to validate the solution set, the factors were correlated with reference spectra and ancillary data (Fig. S47), as discussed below. The five factors were therefore identified as LV-OOA, SV-OOA, COA, HOA, and an unknown factor.

Rotational ambiguity was explored through the fPeak value, where changes resulted in negligible difference in correlation between the mass spectra and time series with reference spectra and ancillary data, respectively. Although there was a change in mass fraction of each factor with different fPeaks (Table S14), this solution space was found to be relatively stable and produced good separation of the factors. Therefore, similarly to the winter IOP, the most central solution (fPeak=0) was chosen as this produced the lowest Q/Q_{exp} value and is most likely to be physically meaningful according to Paatero et al. (2002).

Table S14. Average mass concentration of each of the 5 factors for different fPeak values.

	Factor				
fPeak value	LV-OOA	SV-OOA	Unknown	COA	HOA
-0.8	1.17517	2.07502	1.16182	1.25825	0.368489
0	0.777415	2.27058	1.04627	1.30743	0.640502
1	0.616691	1.82052	1.56815	1.29725	0.738574

LV-OOA correlates strongly with reference spectra, yielding a Pearson's r value of 0.78 with the LV-OOA spectrum from Ng et al. (2011) and 0.94 with Mohr et al. (2012). The lack of a pronounced diurnal pattern and good correlation of the time series with SO_4 (r=0.84) supports the interpretation of this factor as being a well-aged, regional secondary organic aerosol (Jimenez et al., 2009; Lanz et al., 2007).

SV-OOA correlates with reference spectra, yielding a Pearson's r value of 0.79 (Mohr et al., 2012) and 0.92 (Ng et al., 2011). The time series correlates with particulate NO_3 (r=0.44), indicating its semi-volatile characteristics, however the correlation is weaker than for SO_4 (r=0.61). The difference between the time series of SV-OOA factor and NO_3 suggests that the gas-to-particle partitioning is

perhaps not the main driver for the temporal evolution of SV-OOA but rather local emissions and dynamics.

COA correlates with the mass spectral profile of COA from Mohr et al. (2012) with an r of 0.86, and the time series correlates with org55 (r=0.85). The diurnal pattern of COA exhibits a small increase in mass at midday with a very large increase in the evening, peaking at 21:00, corresponding to typical meal times.

The unknown factor, which will be discussed in a future publication, correlates very strongly with mass spectral profiles BBOA (r=0.91) and COA (r=0.87) from Mohr et al. (2012) and the time series correlates with org60 (r=0.60) and org55 (r=0.51). Interestingly, the increase in mass occurs as the COA mass starts to decrease after its peak at 21:00. This can be observed in the time series where the peaks in the COA profile occur in the evening and the peaks in the unknown factor occur shortly afterwards. Also, these peaks are greatest between the start of the measurement period and 28 July as well as from 9 August until the end of the campaign. This trend is similar to that of temperature, where the warmest temperatures are during these two periods.

HOA correlates extremely strongly with reference spectra (r=0.97 Mohr et al., 2012; r=0.95 Ng et al., 2011). A Pearson's r value of 0.85 is yielded when the time series of HOA is correlated with org57, with weaker correlations with combustion tracers CO (r=0.61) and NO_x (r=0.71). The diurnal pattern of HOA exhibits two peaks at 07:00 and 21:00, which correspond to the morning and evening rush hours.

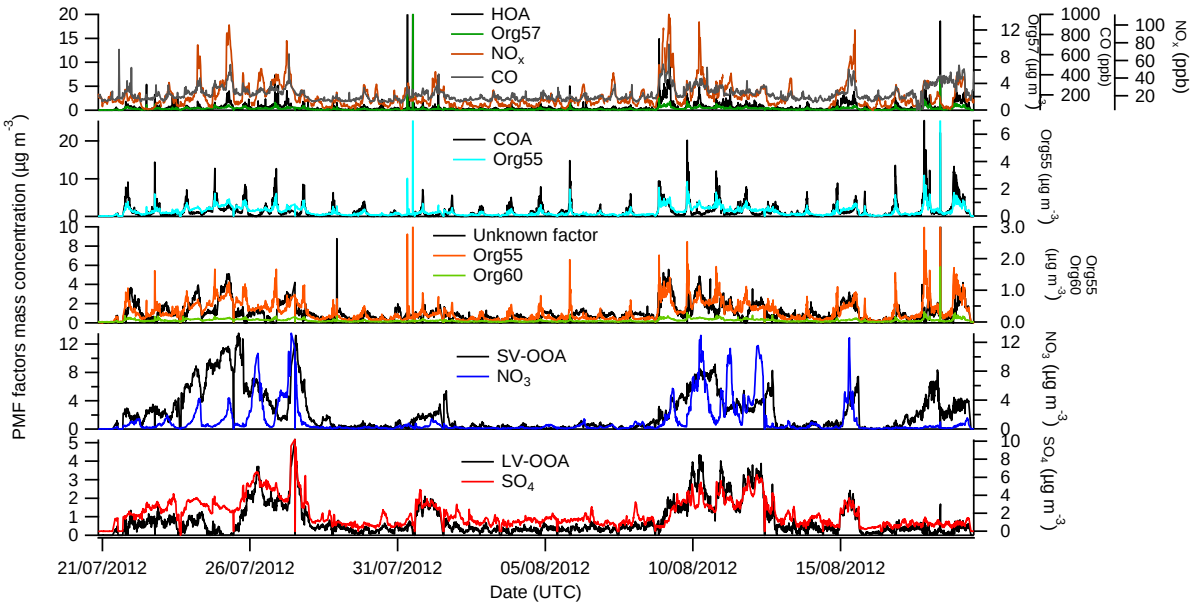

Figure S47. Time series of the 5-factor solution and ancillary data.

6 Comparison of chosen PMF solutions from cToF-AMS and HR-ToF-AMS

To increase confidence in the factorisation of the cToF-AMS, the mass spectra were compared to those from the HR-ToF-AMS PMF from both winter and summer IOPs (Fig. 48 a-g). As the summer period was omitted from the cToF-AMS PMF solution, only the time series from the winter IOP were compared between the solutions from the two instruments (Fig. 48 h-p).

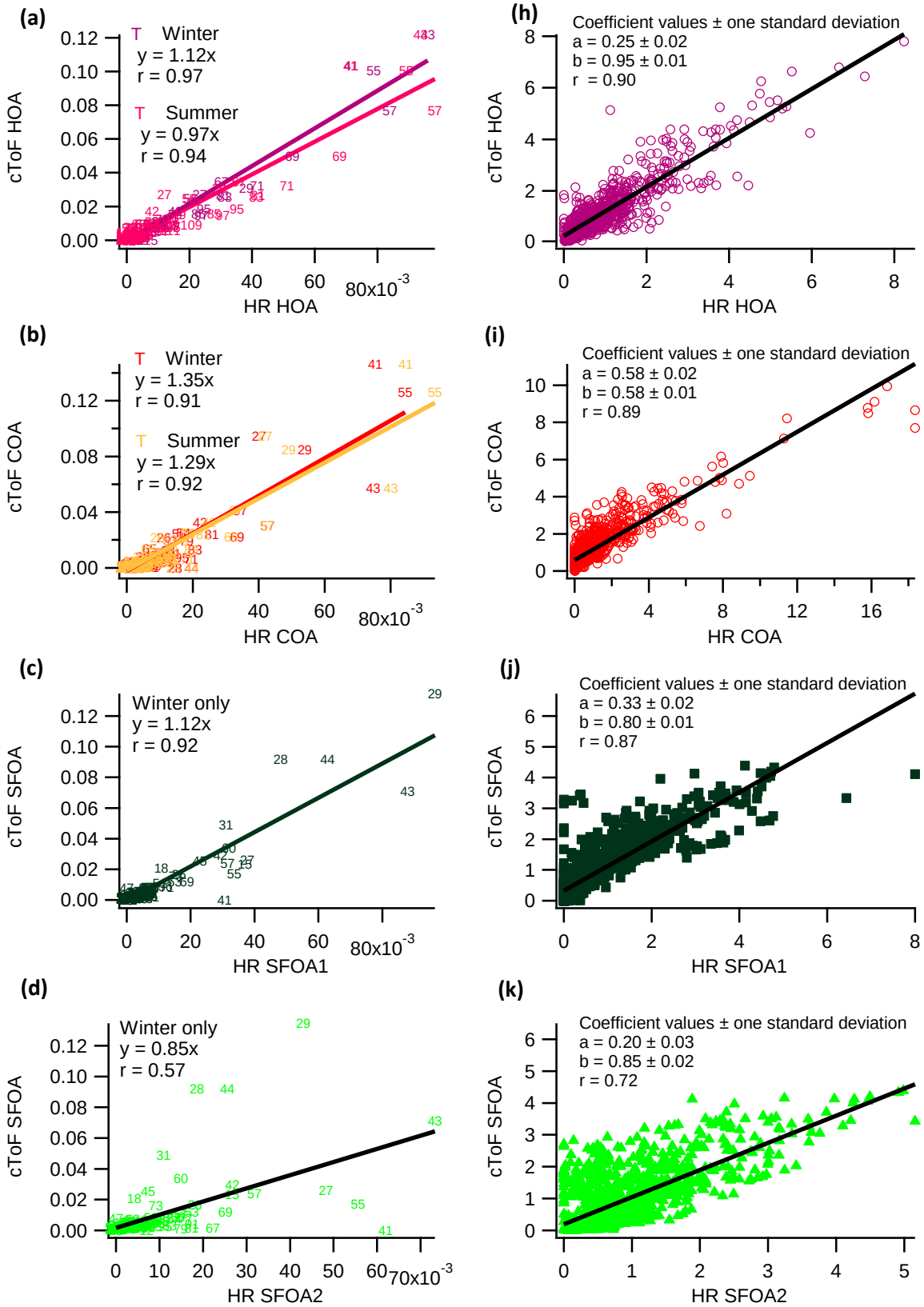
(a)
T Winter
y = 1.12x
r = 0.97
T Summer
y = 0.97x
r = 0.94
cToF HOA
HR HOA
80x10-3
(h)
Coefficient values ± one standard deviation
a = 0.25 ± 0.02
b = 0.95 ± 0.01
r = 0.90
cToF HOA
HR HOA
(b)
T Winter
y = 1.35x
r = 0.91
T Summer
y = 1.29x
r = 0.92
cToF COA
HR COA
80x10-3
(i)
Coefficient values ± one standard deviation
a = 0.58 ± 0.02
b = 0.58 ± 0.01
r = 0.89
cToF COA
HR COA
(c)
Winter only
y = 1.12x
r = 0.92
cToF SFOA
HR SFOA1
80x10-3
(j)
Coefficient values ± one standard deviation
a = 0.33 ± 0.02
b = 0.80 ± 0.01
r = 0.87
cToF SFOA
HR SFOA1
(d)
Winter only
y = 0.85x
r = 0.57
cToF SFOA
HR SFOA2
70x10-3
(k)
Coefficient values ± one standard deviation
a = 0.20 ± 0.03
b = 0.85 ± 0.02
r = 0.72
cToF SFOA
HR SFOA2

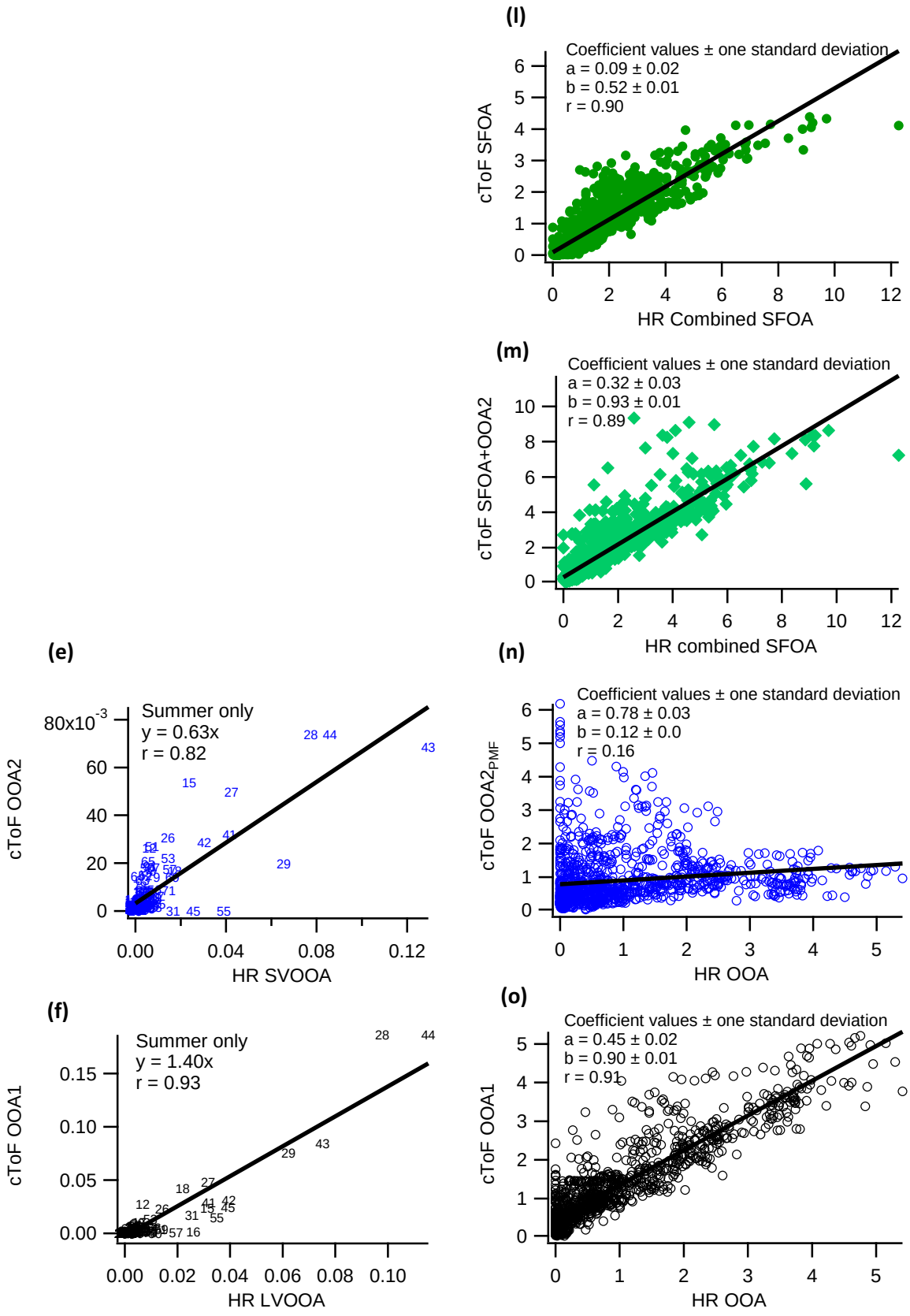
(l)
Coefficient values ± one standard deviation
a = 0.09 ± 0.02
b = 0.52 ± 0.01
r = 0.90
cToF SFOA
HR Combined SFOA
(m)
Coefficient values ± one standard deviation
a = 0.32 ± 0.03
b = 0.93 ± 0.01
r = 0.89
cToF SFOA+OOA2
HR combined SFOA
(e)
Summer only
y = 0.63x
r = 0.82
80x10-3
cToF OOA2
HR SVOOA
(n)
Coefficient values ± one standard deviation
a = 0.78 ± 0.03
b = 0.12 ± 0.0
r = 0.16
cToF OOA2PMF
HR OOA
(f)
Summer only
y = 1.40x
r = 0.93
cToF OOA1
HR LVOOA
(o)
Coefficient values ± one standard deviation
a = 0.45 ± 0.02
b = 0.90 ± 0.01
r = 0.91
cToF OOA1
HR OOA

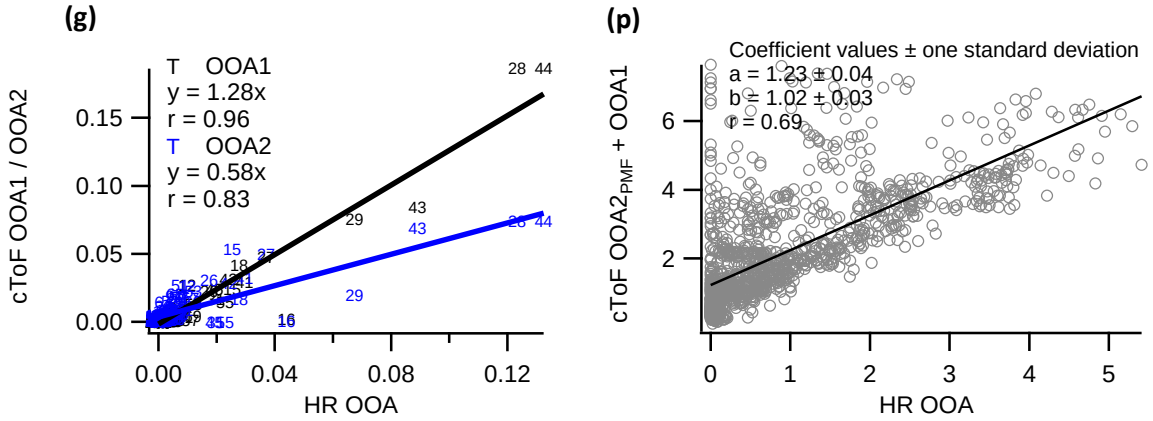

Figure S48. Comparison of the long-term cToF-PMF factors and IOP HR-PMF factors. Plots a-e are mass spectra and f-p are time series. Two SFOA factors were identified from the winter HR-PMF, with no SFOA factors in the summer HR-PMF. Also, it was not possible to separate the OOA factor in to the two subtypes from the winter HR-PMF. Finally, the summer period has been excluded from the long-term cToF-PMF and so there are no time series comparisons for the summer.

References

Alfarra, M. R., Prevot, A. S. H., Szidat, S., Sandradewi, J., Weimer, S., Lanz, V. A., Schreiber, D., Mohr, M., and Baltensperger, U.: Identification of the mass spectral signature of organic aerosols from wood burning emissions, Environ. Sci. Technol., 41, 5770–5777, 2007.

Allan, J. D., Williams, P. I., Morgan, W. T., Martin, C. L., Flynn, M. J., Lee, J., Nemitz, E., Phillips, G. J., Gallagher, M. W., and Coe, H.: Contributions from transport, solid fuel burning and cooking to primary organic aerosols in two UK cities, Atmos. Chem. Phys., 10, 647–668, doi:10.5194/acp-10-647-2010, 2010.

Crippa, M., DeCarlo, P. F., Slowik, J. G., Mohr, C., Heringa, M. F., Chirico, R., Poulain, L., Freutel, F., Sciare, J., Cozic, J., Di Marco, C. F., Elsasser, M., Nicolas, J. B., Marchand, N., Abidi, E., Wiedensohler, A., Drewnick, F., Schneider, J., Borrmann, S., Nemitz, E., Zimmermann, R., Jaffrezo, J.-L., Prévôt, A. S. H., and Baltensperger, U.: Wintertime aerosol chemical composition and source apportionment of the organic fraction in the metropolitan area of Paris, Atmos. Chem. Phys., 13, 961-981, doi:10.5194/acp-13-961-2013, 2013.

Cross, E. S., Slowik, J. G., Davidovits, P., Allan, J. D., Worsnop, D. R., Jayne, J. T., Lewis, D. K., Canagaratna, M., and Onasch, T. B.: Laboratory and ambient particle density determinations using light scattering in conjunction with aerosol mass spectrometry, Aerosol Sci. Tech., 41, 343–359, 2007.

Dall'Osto, M., Ovadnevaite, J., Ceburnis, D., Martin, D., Healy, R. M., O'Connor, I. P., Kourtchev, I., Sodeau, J. R., Wenger, J. C., and O'Dowd, C.: Characterization of urban aerosol in Cork city (Ireland) using aerosol mass spectrometry, Atmos. Chem. Phys., 13, 4997-5015, doi:10.5194/acp-13-4997-2013, 2013.

Jimenez, J. L., Canagaratna, M. R., Donahue, N. M., Prevot, A. S. H., Zhang, Q., Kroll, J. H., DeCarlo, P. F., Allan, J. D., Coe, H., Ng, N. L., Aiken, A. C., Docherty, K. S., Ulbrich, I. M., Grieshop, A. P., Robinson, A. L., Duplissy, J., Smith, J. D., Wilson, K. R., Lanz, V. A., Hueglin, C., Sun, Y. L., Tian, J., Laaksonen, A., Raatikainen, T., Rautiainen, J., Vaattovaara, P., Ehn, M., Kulmala, M., Tomlinson, J. M., Collins, D. R., Cubison, M. J., Dunlea, E. J., Huffman, J. A., Onasch, T. B., Alfarra, M. R., Williams, P. I., Bower, K., Kondo, Y., Schneider, J., Drewnick, F., Borrmann, S., Weimer, S., Demerjian, K., Salcedo, D., Cottrell, L., Griffin, R., Takami, A., Miyoshi, T., Hatakeyama, S., Shimono, A., Sun, J. Y., Zhang, Y. M., Dzepina, K., Kimmel, J. R., Sueper, D., Jayne, J. T., Herndon, S. C., Trimborn, A. M., Williams, L. R., Wood, E. C., Middlebrook, A. M., Kolb, C. E., Baltensperger, U., and Worsnop, D. R.: Evolution of organic aerosols in the atmosphere, Science, 326, 1525–1529, 2009.

Lanz, V. A., Alfarra, M. R., Baltensperger, U., Buchmann, B., Hueglin, C., and Prévôt, A. S. H.: Source apportionment of submicron organic aerosols at an urban site by factor analytical modelling of aerosol mass spectra, Atmos. Chem. Phys., 7, 1503–1522, doi:10.5194/acp-7-1503-2007, 2007.

Liu, D., Allan, J. D., Young, D. E., Coe, H. Beddows, D., Fleming, Z. L., Flynn, M. J., Gallagher, M. W., Harrison, R. M., Lee, J., Prévôt, A. S. H., Taylor, J. W., Yin, J., Williams, P. I., and Zotter, P.: Size

distribution, mixing state and source apportionments of black carbon aerosols in London during winter time, in preparation, 2014.

Mohr, C., Huffman, J. A., Cubison, M. J., Aiken, A. C., Docherty, K. S., Kimmel, J. R., Ulbrich, I. M., Hannigan, M., and Jimenez, J. L.: Characterization of primary organic aerosol emissions from meat cooking, trash burning, and motor vehicles with high resolution aerosol mass spectrometry and comparison with ambient and chamber observations, Environ. Sci. Technol., 43, 2443–2449, 2009.

Mohr, C., DeCarlo, P. F., Heringa, M. F., Chirico, R., Slowik, J. G., Richter, R., Reche, C., Alastuey, A., Querol, X., Seco, R., Peñuelas, J., Jiménez, J. L., Crippa, M., Zimmermann, R., Baltensperger, U., and Prévôt, A. S. H.: Identification and quantification of organic aerosol from cooking and other sources in Barcelona using aerosol mass spectrometer data, Atmos. Chem. Phys., 12, 1649-1665, doi:10.5194/acp-12-1649-2012, 2012.

Ng, N. L., Canagaratna, M. R., Jimenez, J. L., Zhang, Q., Ulbrich, I. M., and Worsnop, D. R.: Real-time methods for estimating organic component mass concentrations from aerosol mass spectrometer data. Environ. Sci. Technol., 45, 910-916, 2011.

Paatero, P., Hopke, P. K., Song, X. H., and Ramadan, Z.: Understanding and controlling rotations in factor analytic models, Chemometr. Intell. Lab, 60, 253-264, Doi 10.1016/S0169-7439(01)00200-3, 2002.

Paatero, P. and Hopke, P. K.: Discarding or downweighting high-noise variables in factor analytic models, Anal. Chim. Acta, 490, 277–289, doi:10.1016/s0003-2670(02)01643-4, 2003.

Sueper, D.: ToF-AMS High Resolution Analysis Software – Pika, online available at: http://cires.colorado.edu/jimenez-group/ToFAMSResources/ToFSoftware/PikaInfo/, 2008.

Ulbrich, I. M., Canagaratna, M. R., Zhang, Q., Worsnop, D. R., and Jimenez, J. L.: Interpretation of organic components from Positive Matrix Factorization of aerosol mass spectrometric data, Atmos. Chem. Phys., 9, 2891–2918, doi:10.5194/acp-9-2891-2918, 2009.

Yin, J., Cumberland, S. Harrison, R. M., Allan, J., Young, D., Williams, P., and Coe, H.: Receptor modelling of fine particles in Southern England including comparison of CMB model outputs with AMS-PMF factors, in preparation, 2014.

Zhang, Q., Worsnop, D. R., Canagaratna, M. R., and Jimenez, J. L.: Hydrocarbon-like and oxygenated organic aerosols in Pittsburgh: insights into sources and processes of organic aerosols, Atmos. Chem. Phys., 5, 3289–3311, doi:10.5194/acp-5-3289-2005, 2005.